Contribution from the Department of Chemistry, Harvard University, Cambridge, Massachusetts 02138, and the The City College, City University of New York, New York, New York 10031

Extended Topological Rules for Boron Hydrides. 1. Structures and Relative Energies for the Transient Boron Hydrides B_2H_4, B_3H_7, B_3H_9, B_4H_8, and B_4H_{12}[1]

IRENE M. PEPPERBERG,[2a] THOMAS A. HALGREN,[2b] and WILLIAM N. LIPSCOMB*[2a]

Received December 23, 1975 AIC50910J

Optimal geometries for the transient boron hydrides B_2H_4, B_3H_7, B_3H_9, B_4H_8, and B_4H_{12}, possible intermediates in the pyrolysis of B_2H_6, have been determined at the approximate ab initio PRDDO level and further assessed via ab initio STO-3G, Slater-orbital SCF, 4-31G, and SCF-CI calculations. Structures having one or more formally vacant orbitals are found to be preferred for the systems B_2H_4, B_3H_7, and B_4H_8 which we define as unsaturated.[3] Preferred symmetries and topologies are D_{2d} 0012 (staggered) for B_2H_4, C_{2v} 1103 (staggered) or possibly C_s 2102 for B_3H_7, D_{3h} 3003 for B_3H_9, C_s 2112C [or possibly D_{2h} 0204 (staggered)] for B_4H_8, and D_{4h} 4004 for B_4H_{12}. An extended *styx* and topological formalism is developed in order to incorporate the new structures by allowing up to one vacant orbital per boron atom. The extended rules are also shown to suggest vacant orbital structures which successfully predict observed distortions from the idealized topological structures for the known hydrides, e.g., B_4H_{10}, B_5H_{11}, and $B_3H_8^-$. Bonding patterns in the transient boron hydrides are characterized via molecular orbital localizations using the criteria of Boys and, in one case, Edmiston–Ruedenberg; and relative energies are discussed in terms of competing tendencies to maximize valency (as defined in ref 17) and to minimize strain. An equation is presented which relates the relative energies for the transient boron hydrides to the differences in their valencies and in their topologies; the root-mean-square deviation between the predicted and observed (4-31G) relative energies is ~5 kcal/mol. Nonlinear BHB bridges in the polyhedral boranes are found to be strained to the extent of ~10 kcal/mol. Finally, additional justification is provided for the exclusion of open BBB bonds from the topological formalism for the boron hydrides.

Although the pyrolysis of diborane has been the subject of several studies,[4] only the initial step, the dissociation of diborane, has undergone detailed theoretical analysis.[5] While the proposed mechanisms[4,6] for formation of the higher boranes substantially agree on a likely set of reaction intermediates, little is known about the transient boron hydrides which presumably serve in this capacity. Accordingly, we present here a computational study of the structures and energies of the transient hydrides B_2H_4, B_3H_7, B_3H_9, B_4H_8, and B_4H_{12}.

Geometries of candidate structures have been optimized using the approximate ab initio method of partial retention of diatomic differential overlap (PRDDO),[7] and relative energies have then been reassessed via individual minimal-basis STO-3G[8] and extended-basis 4-31G calculations.[8] In addition, ab initio SCF[9] and SCF-CI calculations, using minimum-basis sets of Slater orbitals, have been performed on all B_2H_4 and B_3H_7 and some B_4H_8 structures in order to assess the effects of electron correlation. Finally, localized orbital techniques[10-12] have been employed to characterize the bonding in the optimized structures.

Interestingly, the most stable structures for the unsaturated[3] hydrides B_2H_4, B_3H_7, and B_4H_8 were found, like BH_3,[13] to have one or more formally vacant boron p orbitals, in violation of the usual *styx* rules[14] and topological formalism.[14,15] However, modification of the rules along the lines suggested by Dupont and Schaeffer for B_4H_8,[16] to allow up to one vacant orbital per boron, produced an extended scheme rigorously obeyed by all of the optimized structures.

For structures differing only in the orientation of the BH_2 groups which bear vacant orbitals energy differences were found to closely parallel differences in the computed Armstrong–Perkins–Stewart valency[17] and to be partly, but not wholly, derived from changes in the utilization of the formally vacant p orbital(s). Furthermore, both the relative energies and detailed geometries of vacancy and nonvacancy structures for B_2H_4, B_3H_7, and B_4H_8 could be understood in terms of opposing tendencies to maximize valency and to minimize geometric strain. For example, the nonvacancy structures consistently developed strain-relieving bridge-hydrogen asymmetries by incorporating some of the character of companion vacancy structures having terminal hydrogens in place of the hydrogen bridges. The less highly bridged vacancy structures, in contrast, achieved stability by attaining somewhat higher total valencies than expected on topological grounds. As a result, smaller differences in valency were found between vacancy and nonvacancy structures than might have been expected on the basis of the formal vacancy numbers. The relative energies of isomeric structures were found to be reproduced to within a root-mean-square deviation of ~5 kcal/mol by a simple additive relationship based on the difference in total valency and in the numbers of BHB and BBB bonds.

The principal objective of this paper will be to present and to demonstrate the utility of the extended topological formalism for predicting structures and interpreting the stabilities of small boron hydrides. Accordingly, we shall begin by first discussing the vacancy-modified *styx* and topological rules and by then characterizing the structures for various small boron hydrides allowed under the new rules.

Extended *styx* Rules and Topological Formalism

The *styx* rules[14] and the topological formalism[14,15] comprise a set of abstractions of structural principles which provide a means for systematizing known structures and for generating plausible new structures for boron hydrides. Modifications have extended the original scheme to, for example, negative ions[18] and the carboranes.[15,19,20] Similarly, Dupont and Schaeffer some time ago described the modification needed to accommodate a single-vacancy structure for B_4H_8.[16] Our studies independently led us to a more generalized set of vacancy-modified *styx* and topological rules which we shall now present and illustrate. Some initial applications to structural aspects of known, stable boron hydrides are summarized in the Appendix.

Formally, a nonvacancy structure for a *styx* compound B_pH_{q+p}, such as 2102 B_3H_7, can be converted into a single-vacancy structure (a) by converting one of the s BHB bonds into a B–H bond (originally $p + x$ in number) or (b) converting one of the t BBB bonds into a B–B bond (originally y in number) (see eq 1). In either case, one three-center bond is converted into a two-center bond, and the boron omitted from the three-center bond becomes the vacancy center, B^v. Topologically, then, this center will take part in three, rather than the usual four,[21] bonds of the four types just enumerated;

Table I. *s, t, y, x* and *υ* Values[a] for Some B_pH_{p+q} Hydrides

	BH_3	B_2H_4[b]	B_3H_7[b]	B_3H_9	B_4H_8	B_4H_{12}
$\upsilon=0$		(2010)	(3011)	3003	4020	4004
			2102		2202	
					3111	
$\upsilon=1$	0002	(1011)	2012		3021	
			1103		2112	
					1203	
$\upsilon=2$		0012	(1013)		2022	
			0104		1113	
					0204	

[a] *s* = no. of hydrogen bridge bonds, BHB; *t* = no. of boron three-center bonds, BBB; *y* = no. of boron-boron single bonds, B–B; *x* = no. of extra terminal H atoms on B–H, e.g., BH_2 groups; *υ* = no. of vacant boron p orbitals. $s+x=q, s+t+\upsilon=p, t+y+q/2=p$. [b] *styx* values having no topologically allowed structures under the new rules are shown in parentheses.

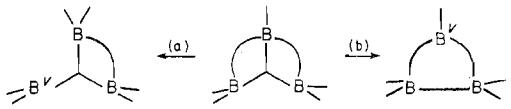

1103 2102 2012 (1)

other topological rules (e.g., that all pairs of adjacent borons be connected by at least a B–B, BHB, or BBB bond) will remain unchanged. Therefore it follows that the modified *styx* rules for a structure containing *υ* vacant orbitals can be written as

$$s+x=q \tag{2}$$

$$s+t=p-\upsilon \tag{3}$$

$$t+y=p-q/2 \tag{4}$$

Thus, the number of three-center bonds, $s+t$, is reduced by the number of vacancies, *υ*, but the numbers of "extra" hydrogens, $s+x$, and of framework bonds, $t+y$, are unchanged.

The inductive process specified in eq 1 relates *styx* values for $\upsilon=1$ structures to the precursor $\upsilon=0$ values,[14a] $\upsilon=2$ values to those for $\upsilon=1$, and so on. The *styx* values for $\upsilon \leq 2$ obtained in this way for B_2H_4, B_3H_7, B_3H_9, B_4H_8, and B_4H_{12} are shown in Table I, and the corresponding topological structures are depicted in Figure 1. We note that the same process can also be employed to generate some, but not all, of the vacancy structures from their nonvacancy precursors. Provisionally, we shall restrict our attention to structures having only central BBB bonds. Structures having open BBB bonds will be considered in the final section of this paper. We note that certain *styx* designations allowed under the new rules yield several acceptable topological structures, while others yield none. For example, the 2010 and 1101 structures for B_2H_4 shown in Figure 1 actually are topologically disallowed, because both two- and three-center bonds connect adjacent borons. However, we include 2010 B_2H_4 in our subsequent discussions for reasons which will become evident. The nonvacancy 2202B structure of B_4H_8, which will also be considered below, represents a second special topological case, in that two BBB bonds and a BHB bond connect a single pair of borons.

In order to reduce the task of determining the most stable structures for each system to one of more manageable fiscal proportions, we shall insist that each candidate structure considered below have one or more pairs of equivalent boron atoms related via at least a plane, center, or twofold axis of symmetry. All small boron hydrides presently known have such symmetry,[15a,22] apparently for good reason. For example, symmetrical formation of B_2H_6 from BH_3 subunits[5,23] allows each subunit to serve as both donor and acceptor, thereby avoiding an unacceptable accumulation of electronic charge on either subunit. *One* BHB bridge, however, *cannot* be formed in this way. Thus, the unsymmetrical end-on approach

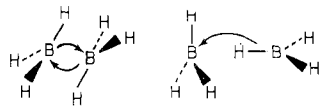

evidently is purely repulsive at the SCF level,[5] as is the similarly one-sided interaction of BH_3 with H_2.[24] As a rule, asymmetric structures seem to have diminished capacities for bonding. We find, for example, that the topologically allowed but asymmetric 3103 form for B_4H_{10} symmetrizes spontaneously during geometry optimization to yield the symmetric 4012 structure.[25] Thus, while 2010 B_2H_4 might conceivably be stable with respect to the open 0012 form, in our estimation the less symmetric 1101 singly bridged structure (Figure 1) definitely would not be.

Thus, the task of determining the most stable structures via geometry optimization, to which we now turn, is less imposing than the number and variety of structures depicted in Figure 1 might first suggest. Moreover, we shall see that relationships between structures akin to those shown in eq 1(a) and 1(b) can be exploited to reduce further the required number of separate geometry optimizations.

Table II. Exponents Used in PRDDO,[a] STO-3G,[b] SCF,[c] and SCF-CI[c] Calculations

B	1s: 4.6838	H_t	1s: 1.1473
	2s: 1.4489	H_b	1s: 1.2095
	2p: 1.4836		

[a] Cf. ref 7. [b] Cf. ref 8. [c] Cf. ref 9.

Geometry Optimizations

In this section, we report the results of PRDDO[7] minimum-basis-set geometry optimizations for B_2H_4, B_3H_7, B_3H_9, B_4H_8, and B_4H_{12} using orbital exponents listed in Table II. All bond angles and internuclear distances, subject to imposed symmetry restrictions, were refined sequentially until consecutive full cycles yielded geometries which differed by less than $\sim 1°$ in bond angles and 0.01 au in bond distances. Optimized coordinates are reported in Table III. Molecular orbital localization results, obtained using the Boys criterion,[10] are summarized in Table IV, and molecular energies are listed in Table V. Ab initio comparisons of relative energies are presented in the next section. Some details of the calculations now follow.

B_2H_4. The 2010 ($\upsilon=0$) and 0012 ($\upsilon=2$) structures shown in Figure 1 were selected for geometry optimization. The former, though topologically disallowed, has been retained to provide an alternative to the $\upsilon=2$ structure and to allow us subsequently to examine the extent of the destabilization which accompanies the topological violation. As shown in Figure 2a and b, both staggered and eclipsed conformations arise for the 0012 structure.

2010. Optimization within D_{2h} symmetry produced a structure (Figure 2c) which contains a B–B π bond and which has uncharacteristically short B–H_t distances, i.e., 2.165 au vs. a normal PRDDO value of 2.19 au.[5]

0012 (ST, EC). Both conformers (ST = staggered; EC = eclipsed), though formally containing two vacant orbitals, were found to lie more than 100 kcal/mol below 2010 B_2H_4 on the PRDDO energy surface (Table V). The staggered form (D_{2d}) was the more stable, and a linear synchronous transit (LST) pathway[26] constructed between the two conformers showed that the higher energy EC conformer (D_{2h}) represents the saddle point (+13.1 kcal/mol) on the rotational potential energy surface.[27] An LST path from the 2010 to the 0012 ST structure also proceeded spontaneously, suggesting that only the latter is an equilibrium geometry in the absence of

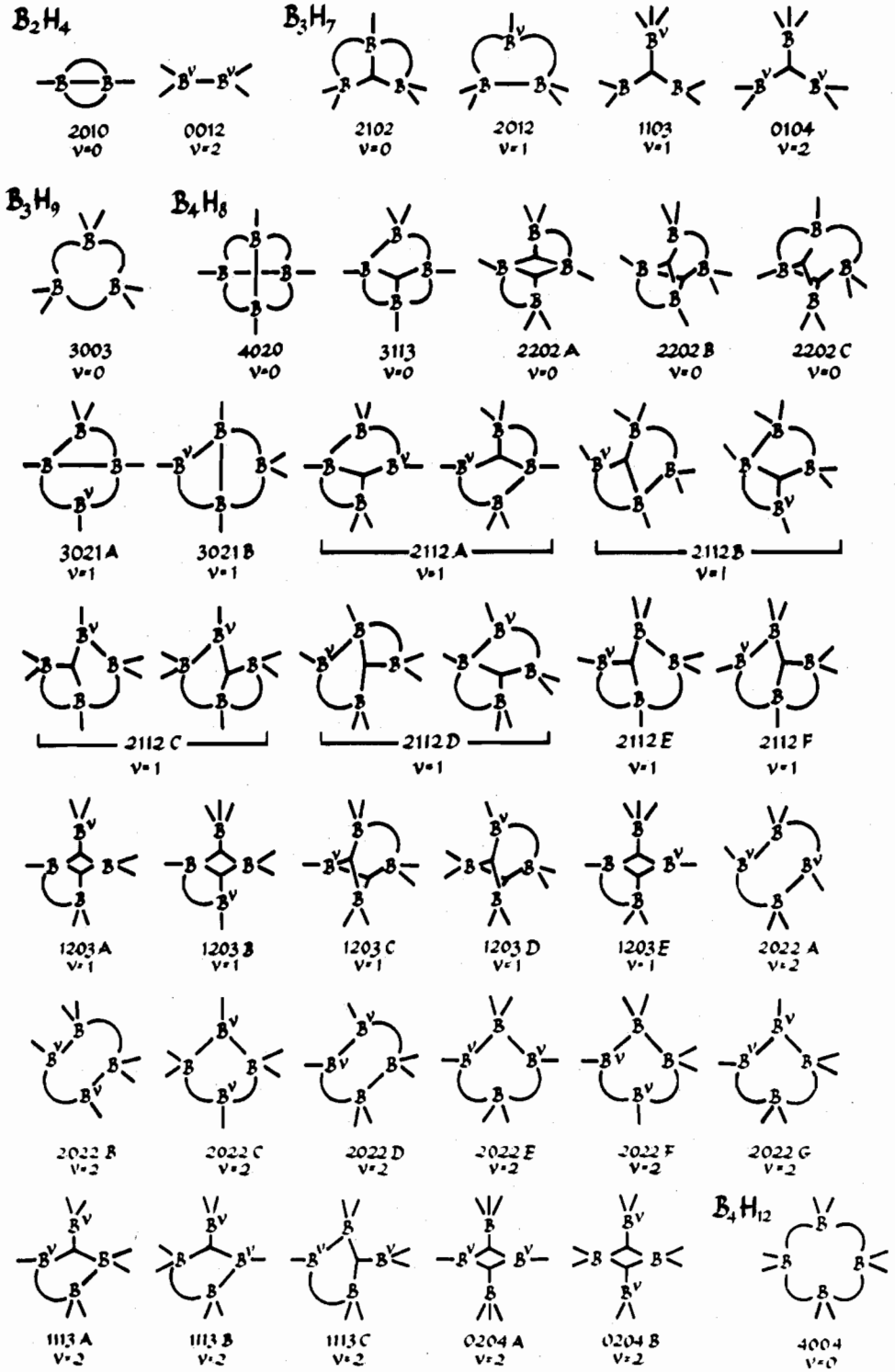

Figure 1. Topologically allowed structures under expanded rules for B_2H_4, B_3H_7, B_3H_9, B_4H_8, and B_4H_{12} having 0, 1, or 2 orbital vacancies, v.

symmetry constraints. Paths can also be constructed between the 2010 and 0012 EC structures which are entirely downhill in energy. However, the approximately least motion LST path,[26] in which a plane of symmetry is retained throughout, produced a significant barrier as a result of an inversion between the highest occupied and the lowest unoccupied orbitals at an intermediate point along the path.

B_3H_7. Of the four possible structures shown in Figure 1, only the 2102 ($v = 0$) and 1103 ($v = 1$) structures were explicitly considered for geometry optimization. We note, however, that the 2012 ($v = 1$) and 2102 structures have the same nuclear geometry (a three-center BBB bond is converted into a two-center B–B bond to create the orbital vacancy), and the 0104 structure ($v = 2$) differs from the latter only in the detailed positioning of the bridge hydrogens. Both "staggered" and "eclipsed" conformations arise for the 1103 structure, where the designation specifies the orientation of the mobile BH_2 group with respect to the BH_2 groups on the flanking borons.

2102. Optimization in C_s symmetry (the mirror plane contains B_3 and H_5 in Figure 3a) produced a well-defined structure having distinctly asymmetric BHB bridges (cf. Figures 3a, b; Table IV). This geometry suggests that the observed structure be viewed as a composite intermediate

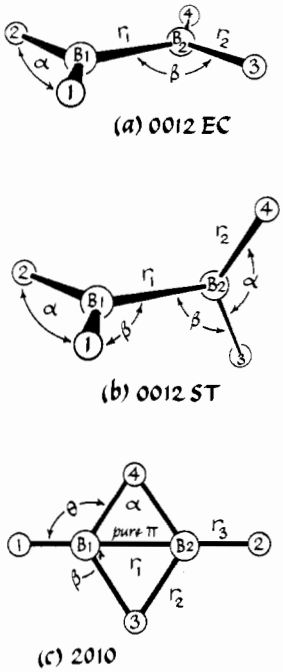

Figure 2. Optimized geometrical and Boys localized valence structures for B_2H_4: (a) 0012 EC, $r_1 = 3.180$ au, $r_2 = 2.210$ au, $\alpha = 117.0°$, $\beta = 121.5°$; (b) 0012 ST, $r_1 = 3.060$ au, $r_2 = 2.210$ au, $\alpha = 117.0°$, $\beta = 121.5°$; (c) 2010, $r_1 = 2.704$ au, $r_2 = 2.468$ au, $r_3 = 2.165$ au; $\alpha = 66.4°$, $\beta = 113.6°$, $\theta = 123.2°$.

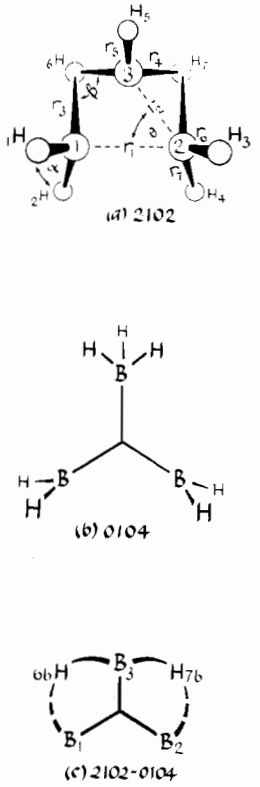

Figure 3. B_3H_7: (a) optimized geometrical structure for 2102; $r_1 = 3.664$ au, $r_2 = 3.147$ au, $r_3 = 2.924$ au, $r_4 = 2.348$ au, $r_5 = 2.188$ au, $r_6 = 2.201$ au, $r_7 = 2.206$ au, $\alpha = 117.3°$, $\beta = 72.4°$, $\theta = 54.4°$, H_5–B_3–$H_6 = 112.7°$, B_1–B_4–$B_3 = 71.2°$; (b) valence structure for the proposed 0104 contribution; (c) Boys localized valence structure for 2102; all terminal hydrogens have been omitted from all of the borons. The bridge bonding legend employed here and in subsequent figures is as follows: dashed curved arrow represents a contribution of 0.1–0.2 e from the B to which the arrow is drawn; solid curved arrow, 0.21–0.3 e; dashed curve, 0.31–0.4 e; and solid curve, >0.41 e.

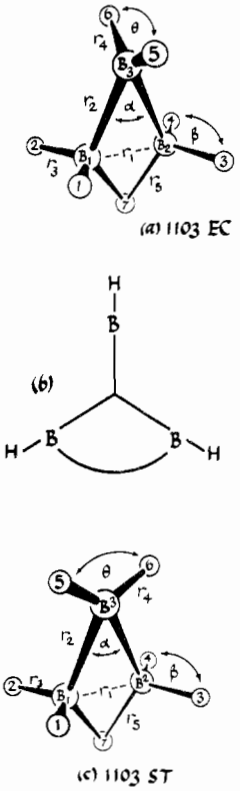

Figure 4. 1103 B_3H_7: (a) optimized geometrical structure for the EC conformer; $r_1 = 3.264$ au, $r_2 = 3.573$ au, $r_3 = 2.201$ au, $r_4 = 2.213$ au, $r_5 = 2.497$, $\alpha = 54.4°$, $\beta = 118.4°$, $\theta = 116.5°$, B_1–B_2–$B_3 = 62.8°$, B_1–H_7–$B_2 = 81.6°$; (b) valence structure for both conformers EC and ST; (c) optimized geometrical structure for the ST conformer; $r_1 = 3.264$ au, $r_2 = 3.432$ au, $r_3 = 2.201$ au, $r_4 = 2.214$ au, $r_5 = 2.497$ au, $\alpha = 56.8°$, $\beta = 116.4°$, $\theta = 112.5°$, B_1–B_2–$B_3 = 61.6°$, B_1–H_7–$B_2 = 81.6°$.

between structures of 2102 ($v = 0$) and 0104 ($v = 2$) topology (Figure 3c). As discussed in detail later, the intermediate geometry can be understood to result from a balance between the greater degree of bonding in the former and the lesser geometric strain of the latter. In addition, the LMO populations show that the 2012 structure is not an important contributor to the bonding, because the BBB bond is very symmetrical (Table IV).

1103 (ST, EC). Both the ST and EC conformations were optimized in C_{2v} symmetry (cf. Figure 4). Each was found to be lower in energy than the 2102 structure, by 12.4 and 3.6 kcal/mol, respectively. Moreover, the LST paths[26] between the 2102 and 1103 ST and also between the 1103 EC and 1103 ST structures displayed monotonic decreases in energy. Evidently, the ST conformer is the only equilibrium geometry, at least on the PRDDO energy surface. The 2102 structure could, however, possibly serve as a low-energy transition state for the exchange of bridge and terminal hydrogens in 1103 B_3H_7.

B_3H_9. Even under the extended formalism, the only admissible topology is 3003. Structures such as 2004 ($v = 1$) or 1005 ($v = 2$) satisfy the modified *styx* rules but are unsatisfactory on topological grounds. Although optimized in C_{2v} symmetry, a well-defined structure of higher D_{3h} symmetry resulted (Figure 5).

B_4H_8. The extended formalism produces no less than 14 structures having at least a plane, center, or twofold axis of symmetry which relates equivalent borons (cf. Figure 1). However, several relationships between structures can be exploited to reduce the required number of optimizations. For example, optimization of the 4020 structure ($v = 0$) in C_2 or C_{2v} symmetry, rather than in D_{4h} or D_{2d}, will allow deformation

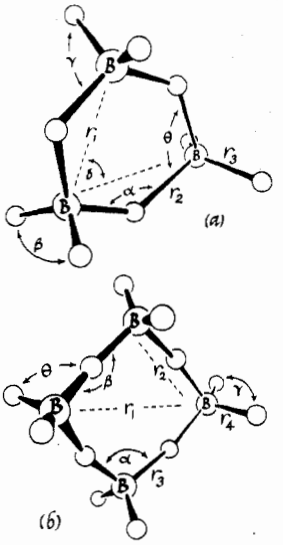

Figure 5. Optimized geometrical and Boys localized valence structures: (a) B_3H_9, $r_1 = 4.377$ au, $r_2 = 2.444$ au, $r_3 = 2.198$ au, $\alpha = 127.1°$, $\beta = 120.1°$, $y = 106.5°$; (b) B_4H_{12}, $r_1 = 6.866$ au, $r_2 = 4.855$ au, $r_3 = 2.437$ au, $r_4 = 2.192$ au, $\alpha = 100.3°$, $\beta = 169.7°$, $\gamma = 120.6°$; $\theta = 108.5°$. Open circles represent hydrogens.

to the 0204A or 0204B ($v = 2$) geometries, respectively, if either deformation is energetically advantageous. Similarly, optimization of the nonvacancy 2202A structure in C_2 symmetry also will permit distortion to either the 0204A or 0204B geometry. Furthermore, as in the case of 2102 and 2012 B_3H_7, the 2112A ($v = 1$) and 2022A ($v = 2$) structures shown in Figure 1 have the same nuclear geometry as the parent $v = 0$ structure, 2202A, and the series 2202B, 2112B, and 2022B is related in the same way. Among the remaining $v = 1$ structures, 2112C and 2112D have the requisite symmetry and are parent structures for 2022C and 2022D, $v = 2$.

Thus, the optimization of the 4020, 2202A and B, and 2112C and D structures will enable us to examine 13 of the 14 symmetrical structures shown in Figure 1. We shall not consider the 2022E structure, which possesses two strained BHB bridges *and* two orbital vacancies.

2202A. Optimization in C_2 symmetry produced a structure having extremely asymmetric BHB bridges (long B–H distance, ~4.2 au).[28] On closer examination, this structure proved to be essentially the 0204B structure ($v = 2$) shown in Figure 1. Accordingly, model "staggered" and "eclipsed" 0204B conformations (cf. Figure 6a and b) were constructed and were optimized in D_{2h} symmetry. The ST conformer was found to lie 11.8 kcal/mol below the EC conformer on the PRDDO energy surface; the EC conformer again represents the point of highest energy on the rotational surface.

2112C. Optimization in C_s symmetry produced a structure having slightly asymmetric BHB bridges (Figure 7a) and lying 6.9 kcal/mol above 0204 ST in energy. The Boys localized orbitals show two fractional[20,29] central BBB bonds (Figure 7b); an alternative description having an open BBB bond is considered in the final section of this paper.

4020. Optimization in C_2 symmetry led to the loss of fourfold symmetry and produced the pronounced bridge asymmetries shown in Figure 8a and b.[30] The detailed LMO results (Table IV) further show that the optimized structure possesses two symmetrical central BBB bonds. As we noted for "2102–0104" B_3H_7, these two factors suggest that the optimized structure be viewed as a composite intermediate between the 4020 ($v = 0$) and 0204A ($v = 2$) topologies shown respectively in Figures 1 and 8c. Optimized synchronous transit pathways[26] from this "4020–0204A" structure to each

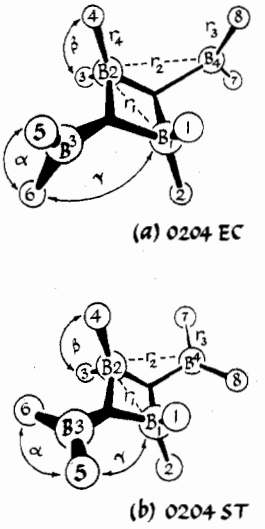

Figure 6. Optimized geometries for 0204B B_4H_8: (a) EC, $r_1 = 3.114$ au, $r_2 = 3.549$ au, B_3–$B_4 = 6.378$ au, $r_3 = 2.213$ au, $r_4 = 2.191$ au, $\alpha = 116.5°$, $\beta = 115.4°$, $\gamma = 118.3°$, B_1–B_3–$B_2 = 52.1°$, B_3–B_2–$B_4 = 127.9°$; (b) ST, $r_1 = 3.184$ au, $r_2 = 3.457$ au, B_3–$B_4 = 6.138$ au, $r_3 = 2.213$ au, $r_4 = 2.201$ au, $\alpha = 112.5°$, H_1–B–$H_2 = 114.4°$, $\gamma = 96.4°$, B_1–B_3–$B_2 = 54.8°$, B_3–B_2–$B_4 = 125.2°$. (a) and (b) also depict the Boys localized valence structures. Legend for boron bonding employed here and in subsequent figures: solid arrow drawn from LMO centroid implies contribution of 0.25–0.35 e; dashed line, 0.35–0.50 e; solid line, >0.5 e (cf. ref 10).

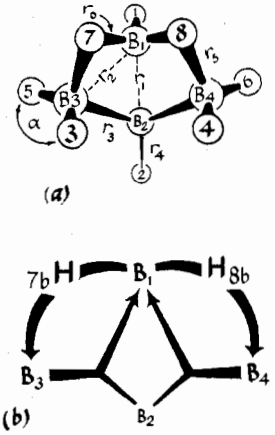

Figure 7. 2112C B_4H_8: (a) optimized geometrical structure; $r_1 = 3.327$ au, $r_2 = 3.516$ au, $r_3 = 3.168$ au, B_3–$B_4 = 5.385$ au, $r_4 = 2.192$ au, $r_5 = 2.907$ au, $r_6 = 2.336$ au, $\alpha = 117.0°$, B_1–B_3–$B_2 = 59.4°$, B_3–B_2–$B_4 = 116.4°$, B_1–H_7–$B_3 = 83.5°$, H_7–B_1–$H_8 = 104.1°$, H_1–B_1–$H_7 = 113.8°$; (b) localized (Boys and ER) structure. All terminal hydrogens have been omitted.

of the lower energy 0204 ST, 0204 EC, and 2112C structures entailed no energy barrier for formation of the latter structures. Although the intermediate structure is therefore not an equilibrium geometry on the PRDDO energy surface, it is, however, a possible transition state for exchange of hydrogen atoms between the pairs of distinct BH_2 groups in the 0204 ST or EC conformer (cf. Figure 9) and also for interconversion of the 2112C and 0204 ST structures.[31]

2202B. Optimization in C_{2v} symmetry produced a well-defined structure (Figure 10) which was, like the "4020–0204A" structure, some 42 kcal/mol above 0204 ST on the PRDDO energy surface. Further optimization in the lower C_2 or C_s point group anticipated for the related $v = 1$ and v

Table III. Optimized Coordinates[a] for Unique Centers

			$\hat{x}$	$\hat{y}$	$\hat{z}$
B_2H_4	2010	$H1_t$	3.517 15	0.0	0.0
			3.574 44[b]	0.0	0.0
		$H3_b$	0.0	2.064 71	0.0
		B1	1.352 15	0.0	0.0
	0012 EC	$H1_t$	2.744 86	0.0	1.884 34
			2.770 99[b]	0.0	1.926 97
		B1	1.590 15	0.0	0.0
	0012 ST	$H1_t$	2.684 86	0.0	1.884 34
			2.710 98[b]	0.0	1.926 97
		$H3_t$	2.684 86	1.884 34	0.0
			2.710 98[b]	1.926 97	0.0
		B1	1.530 15	0.0	0.0
B_3H_7	2102	$H1_t$	3.102 40	0.062 89	1.796 16
			3.130 76[b]	0.064 29	1.836 26
		$H3_t$	2.252 74	1.469 62	−1.590 06
			2.261 19[b]	1.499 15	1.622 01
		$H5_t$	0.0	−4.079 13	1.573 60
			0.0[b]	−4.122 20	1.618 17
		$H6_b$	1.947 77	−2.612 02	−1.310 00
		B1	1.832 10	0.0	0.0
		B3	0.0	−2.558 86	0.0
	1103 EC	$H1_t$	2.759 05	0.032 37	1.890 18
			2.784 20[b]	0.033 09	1.932 37
		$H5_t$	0.0	−4.343 84	1.881 04
			0.0[b]	−4.363 54	1.912 86
		$H7_b$	0.0	1.890 00	0.0
		B1	1.632 10	0.0	0.0
		B3	0.0	−3.178 86	0.0
	1103 ST	$H1_t$	2.784 63	0.133 32	1.870 23
			2.810 35[b]	0.136 30	1.911 98
		$H5_t$	1.839 24	−4.248 78	0.0
			1.870 35[b]	−4.269 58	0.0
		$H7_b$	0.0	1.890 00	0.0
		B1	1.632 10	0.0	0.0
		B3	0.0	−3.018 86	0.0
B_3H_9	3003[c]	$H1_t$	3.139 15	1.812 37	1.904 39
			3.207 75[b]	0.612 07	1.884 75
		$H5_t$	0.0	−3.624 77	1.904 39
			0.0[b]	−4.612 07	1.903 44
		$H7_b$	2.071 77	−2.442 02	0.0
			2.036 80	−1.175 93	0.0
		$H9_b$	0.0	1.162 02	0.0
			0.0	2.351 88	0.0[b]
		B1	2.142 10	0.0	0.0
			2.188 25	1.263 38	0.0[b]
		B3	0.0	−3.748 49	0.0[b]
			0.0	−2.526 78	0.0[b]
B_4H_8	2202B	$H1_t$	3.506 26	1.810 20	0.0
		$H3_t$	1.810 73	−1.701 56	3.012 02
		$H7_b$	0.0	3.366 83	0.0
		$H8_b$	0.0	−2.990 53	0.0
		B1	1.400 30	1.258 36	0.0
		B3	0.0	−1.259 36	1.858 33
	"4020-0204A"	$H1_t$	3.335 00	0.0	−1.234 29
		$H3_t$	0.0	4.600 57	0.574 95
		$H5_b$	1.837 95	2.127 22	2.689 06
		B1	1.523 54	0.0	0.0
		B3	0.0	2.577 44	1.418 89
	2112C	$H1_t$	2.657 63	0.0	−2.095 35
			2.674 64[b]	0.0	−2.150 69
		$H2_t$	−3.457 32	0.0	−0.457 32
			−3.514 03[b]	0.0	−0.469 41
		$H3_t$	−0.575 18	2.877 37	3.136 11
			−0.590 37[b]	2.882 25	3.191 74
		$H5_t$	0.196 34	4.550 71	−0.117 24
			0.201 53	4.599 79	−0.147 51
		$H7_b$	2.772 95	1.842 22	1.219 06
		B1	2.013 54	0.0	0.0
		B2	−1.313 54	0.0	0.0
		B3	0.0	2.692 44	1.028 89
	0204 EC	$H1_t$	2.728 47	0.0	1.851 59
			2.760 01[b]	0.0	1.901 45
		$H5_t$	0.0	−4.353 84	1.881 04
			0.0[b]	−4.381 44	1.925 61
		B1	1.557 10	0.0	0.0
		B3	0.0	3.188 86	0.0
	0204 ST	$H1_t$	2.784 99	0.0	1.849 69
			2.811 55[b]	0.0	1.890 88
		$H5_t$	1.839 24	−4.298 78	0.0
			1.874 50[b]	−4.322 36	0.0
		B1	1.592 10	0.0	0.0
		B3	0.0	3.068 86	0.0
B_4H_{12}	4004	$H1_t$	4.519 84	0.0	1.903 57
			4.548 60[b]	0.0	1.953 94
		$H5_t$	0.0	4.519 84	1.903 57
			0.0[b]	4.548 60	1.953 94
		$H7_b$	1.870 79	1.870 79	0.0
		B1	3.432 97	0.0	0.0
		B3	0.0	3.432 97	0.0

[a] Unless otherwise noted, these are PRDDO optimized values. [b] These values correspond to B–H_t bonds lengthened by 0.06 au to account for the consistent small shortening of PRDDO optimized B–H_t bond lengths (cf. ref 5). These coordinates have been employed in the SCF and SCF-CI calculations. [c] PRDDO coordinates are in a slightly different orientation with respect to the origin. The SCF optimizations were carried out to within 0.005 Å of D_{3h} symmetry. Later PRDDO optimizations showed that D_{3h} symmetry was achieved with a difference of ~2 kcal/mol relative to that obtained for the SCF geometry.

= 2 structures, 2112B and 2202B, produced no change in energy or geometry. The localized orbitals (Table IV) display the symmetrical three-center BBB bonds expected for the parent structure. Interestingly, the B_2H_5 and B_2H_3 fragments of the optimized structure are very similar to the corresponding fragments in B_2H_6 and 2010 B_2H_4, respectively. Optimized synchronous transit pathways[26] failed to yield spontaneous conversions to the lower energy 0204 ST, 0204 EC, or 2112C structures, suggesting that the 2202B structure is an equilibrium geometry on the PRDDO energy surface.

2112D. Optimization in C_s symmetry of an initial structure obtained by juxtaposing one B_2H_4 subunit taken from 2102 B_3H_7 and a second based on 0012 EC B_2H_4 lead, ultimately, to dissociation to two B_2H_4 groups. A probable reason for this behavior is discussed in a later section.

B_4H_{12}. Optimization of a structure of 4004 topology in C_{2v} symmetry produced a well-defined structure (Figure 5b) of higher D_{4h} symmetry. As was the case for 3003 B_3H_9, this topology is the only topology admissible even under the extended formalism.

Comparison of Relative Energies

In Tables V and VI we report ab initio energies for minimum-basis-set Slater-orbital (denoted simply "SCF" for convenience),[9] STO-3G,[8] and extended-basis-set 4-31G[8] calculations on the PRDDO optimized structures discussed above. The Slater-orbital SCF and the STO-3G calculations test specific PRDDO approximations, while the 4-31G calculations examine the adequacy of the minimum-basis-set (MBS) approximation. Also reported are configuration interaction calculations (SCF-CI) based on all single and double excitations constructed from the MBS SCF orbitals, using Stevens' program.[9] The CI corrections might, of course, be substantially different if an extended basis set were used.

Table IV. Boys Localized Orbitals

	Structure	LMO A–B–C	Populations A	B	C	% d^a
B_2H_4	2010	B1 (2)[b]	2.01			2.96
		B1–H1 (2)	0.96	1.05		5.76
		B1–B2 (1)	1.00	1.00		0.00
		B1–H_b–B1 (2)	0.56	0.89	0.56	9.22
	0012 EC	B1 (2)	2.01			2.83
		B1–H1 (4)	0.89	1.13		6.90
		B1–B2 (1)	1.02	1.02		9.55
	0012 ST	B1 (2)	2.01			2.93
		B1–H1 (4)	0.89	1.11		6.55
		B1–B2 (1)	1.02	1.02		9.68
B_3H_7	2102	B1 (2)	2.01			3.00
		B3 (1)	2.01			3.45
		B1–H1 (2)	0.92	1.09		9.01
		B1–H3 (2)	0.93	1.09		9.61
		B3–H5 (1)	0.94	1.08		9.35
		B1–H_b–H3 (2)	0.31	1.00	0.71	11.47
		B1–B2–B3 (1)	0.68	0.68	0.69	16.01
	1103 EC	B1 (2)	2.01			3.20
		B3 (1)	2.01			2.73
		B1–H1 (4)	0.92	1.10		9.61
		B3–H5 (2)	0.93	1.09		8.29
		B1–H_b–B2 (1)	0.52	0.99	0.52	11.97
		B1–B2–B3 (1)	0.60	0.60	0.85	14.91
	1103 ST	B1 (2)	2.01			3.27
		B3 (1)	2.01			2.83
		B1–H1 (4)	0.91	1.10		9.92
		B3–H5 (2)	0.94	1.04		8.77
		B1–H_b–B2 (1)	0.52	1.00	0.52	12.52
		B1–B2–B3 (1)	0.57	0.57	0.90	14.66
B_3H_9	3303	B1 (3)	2.01			3.05
		B1–H1 (6)	0.92	1.09		9.77
		B1–H_b–B3 (3)	0.47	1.09	0.47	12.00
B_4H_8	2202B	B1 (2)	2.01			3.24
		B3 (2)	2.01			3.31
		B1–H1 (2)	1.00	1.01		8.86
		B3–H3 (4)	0.91	1.06		10.93
		B1–$H7_b$–B2 (1)	0.55	0.91	0.55	12.15
		B3–$H8_b$–B4 (1)	0.51	1.04	0.51	13.07
		B1–B2–B3 (2)	0.66	0.66	0.72	13.04
	"4020–0204A"	B1 (2)	2.01			3.01
		B3 (2)	2.01			3.61
		B1–H1 (2)	0.98	1.03		8.67
		B3–H3 (2)	0.91	1.09		9.08
		B1–H_b–B3 (4)	0.20	1.01	0.78	13.47
		B1–B2–B3 (2)	0.66	0.66	0.70	16.86
	2112C	B1 (1)	2.01			3.26
		B2 (1)	2.01			3.02
		B3 (2)	2.01			3.14
		B1–H1 (1)	0.94	1.07		10.16
		B2–H2 (1)	0.96	1.01		9.02
		B3–H3 (2)	0.89	1.10		10.47
		B3–H5 (2)	0.91	1.10		9.21
		B1–H_b–B3 (2)	0.73	1.10	0.29	12.51
		B1–B2–B3 (2)	0.28	0.95	0.79	15.48
	0204 EC	B1 (2)	2.01			3.33
		B3 (2)	2.01			2.71
		B1–H1 (4)	0.91	1.10		10.00
		B3–H5 (4)	0.93	1.09		8.43
		B1–B2–B3 (2)	0.61	0.61	0.81	15.18
	0204 ST	B1 (2)	2.01			3.35
		B3 (2)	2.01			2.79
		B1–H1 (4)	0.90	1.10		10.79
		B3–H5 (4)	0.94	1.05		8.77
		B1–B2–B3 (2)	0.58	0.58	0.87	15.35
B_4H_{12}	4004	B1 (4)	2.01			3.05
		B1–H1 (8)	0.92	1.10		9.32
		B1–H_b–B3 (4)	0.44	1.16	0.44	12.27

[a] $d = [\frac{1}{2}\int(\phi - \phi^T)^2\, d\tau]^{1/2}$, the delocalization, where ϕ is an LMO and ϕ^T is obtained from ϕ by truncating nonlocal contributions and renormalizing; cf ref 10. [b] Number of equivalent atoms or bonds present.

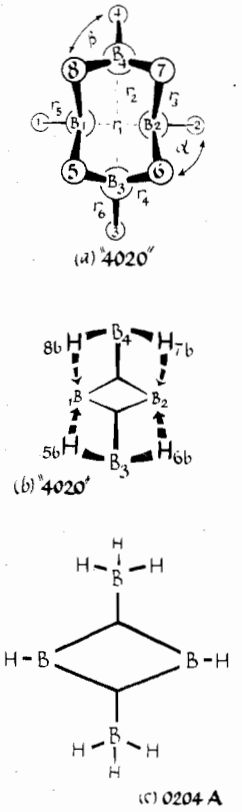

Figure 8. B_4H_8: (a) optimized geometrical structure for "4020"; r_1 = 3.047 au, r_2 = 5.142 au, B_1–B_3 = 3.216 au, r_3 = 3.226 au, r_4 = 2.251 au, r_5 = 2.192 au, r_6 = 2.195 au, α = 109.9°, β = 113.1°, B_1–H_5–B_3 = 69.3°, H_5–B_3–H_6 = 109.5°, B_1–B_3–B_2 = 56.6°, B_3–B_1–B_4 = 106.2°; (b) Boys localized valence structure for "4020"; one terminal hydrogen is omitted for each boron; (c) companion 0204A structure.

Table VI shows that all methods, like PRDDO, find a vacant orbital structure to be the most stable for B_2H_4, B_3H_7, and B_4H_8, though some differences occur in the detailed ordering. In particular, 2112C B_4H_8 falls below 0204 ST in both the 4-31G and SCF-CI calculations. In addition, 2102 B_3H_7 becomes lower in energy than the 1103 EC vacancy structure at the 4-31G and SCF-CI levels, and "4020–0204A" B_4H_8 similarly falls below the 0204 EC conformer on the 4-31G energy surface. This reordering partly reflects a selective stabilization of the more highly bridged structures by 1–3 kcal/mol per BHB bridge upon extension of the basis sets and by 2–4 kcal/mol per bridge upon inclusion of configuration interaction.

A second factor in producing the reordering is a widening of the gap between the ST and EC conformers for B_3H_7 and B_4H_8 in the ab initio MBS calculations. Extension of the basis sets further increases the separation slightly, e.g., by 1.1–2.6 kcal/mol (Table VI), but MBS CI has virtually no net effect. Interestingly, the ST–EC energy difference for 0012 B_2H_4, 12.2–13.1 kcal/mol, is rather insensitive to the method of calculation. Indeed, recent 6-31G* calculations by Dill et al.[27a] and double-ζ calculations by Armstrong[27c] similarly find this energy difference to be 10.5 and 12.2 kcal/mol, respectively. Evidently, certain types of interaction are handled well by all the methods, including PRDDO, while others are not.

Thus, vacant orbital structures remain favored for the three unsaturated[3] hydrides. In view of the separate effects of CI and of extension of the basis sets, however, a large-basis CI calculation might conceivably place 2102 B_3H_7 (v = 0) below the 1103 ST structure. Similarly, the observation that both factors separately place 2112C B_4H_8 below 0204 ST B_4H_8 suggests that 2112C is indeed the form of minimum energy. Our decision, made for economic reasons, to use the PRDDO

Table V. Energetics (au and kcal/mol; 1 au = 627.567 kcal)[a]

	Structure	PRDDO	SCF	STO-3G	4-31G	SCF-CI
B_2H_4	2010	−51.4167	−51.4059	−50.8616	−51.4583	−51.5328
		−32 267.4	−32 260.6	−31 919.0	−32 293.5	−32 340.3
	0012 EC	−51.5996	−51.5448	−50.9989	−51.5381	−51.6287
		−32 382.2	−32 347.8	−32 005.2	−32 343.6	−32 400.5
	0012 ST	−51.6206	−51.5642	−51.0184	−51.5577	−51.6494
		−32 395.3*	−32 360.0*	−32 017.4*	−32 355.9*	−32 413.4*
B_3H_7	2102	−77.9744	−77.9055	−77.0867	−77.9067	−78.0630
		−48 934.1	−48 890.9	−48 377.0	−48 891.7	−48 989.8
	1103 EC	−77.9801	−77.9022	−77.0823	−77.8977	−78.0544
		−48 937.7	−48 888.8	−48 374.3	−48 886.0	−48 984.3
	1103 ST	−77.9942	−77.9220	−77.1026	−77.9197	−78.0738
		−48 946.5*	−48 901.3*	−48 387.0*	−48 899.8*	−48 996.5*
B_3H_9	3003	−79.0977	−79.0470	−78.2246	−79.0463	−79.2124
		−49 639.1	−49 607.3	−49 091.1	−49 606.8	−49 711.0
B_4H_8	2202B	−103.1658		−101.9896	−103.0839	
		−64 743.5		−64 005.2	−64 692.0	
	"4020-0204A"	−103.1671[b]		−101.9879[b]	−103.0838	
		−64 744.2		−64 004.2	−64 691.9	
	2112C	−103.2223	−103.1193	−102.0323	−103.1181	−103.3140
		−64 778.8	−64 714.2	−64 032.1	−64 713.5*	−64 836.4*
	0204 EC	−103.2146	−103.0876	−101.9978	−103.0765	−103.2775
		−64 774.0	−64 694.3	−64 010.4	−64 687.4	−64 813.5
	0204 ST	−103.2332	−103.1215	−102.0326	−103.1155	−103.3104
		−64 785.8*	−64 715.6*	−64 032.2*	−64 711.8	−64 834.1
B_4H_{12}	4004	−105.4542	−105.3901	−104.2863		
		−66 179.5	−66 139.3	−65 446.6		

[a] Asterisks mark the structures of lowest energy for each method. [b] This is the energy obtained with bridge exponents (cf. Table II) for the asymmetric bridge hydrogens.

Table VI. Energies Relative to the ST Isomers (kcal/mol)

	Structure	PRDDO	Δ_1[a]	STO-3G	Δ_2[b]	4-31G	SCF	Δ_3[c]	SCF-CI
B_2H_4	2010	127.9		98.4		62.4	99.4		73.1
			−29.5		−36.0			−26.3	
	0012 EC	13.1		12.2		12.3	12.2		12.9
			−0.9		+0.1			+0.7	
	0012 ST	0.0		0.0		0.0	0.0		0.0
B_3H_7	2102	12.4		10.0		8.1	10.4		6.7
			−2.4		−1.9			−3.7	
	1103 EC	8.8		12.7		13.8	12.5		12.2
			+3.9		+1.1			−0.3	
	1103 ST	0.0		0.0		0.0	0.0		0.0
B_4H_8	2202B	42.4		27.0		19.8			
			−15.4		−7.2				
	"4020-0204A"	41.6		28.0		19.9			
			−13.6		−8.1				
	2112C	7.0		0.1		−1.7	1.4		−2.3
			−6.9		−1.8			−3.7	
	0204 EC	11.8		21.8		24.4	21.3		20.6
			+10.0		+2.6			−0.7	
	0204 ST	0.0		0.0		0.0	0.0		0.0

[a] Δ_1 is the STO-3G energy relative to the PRDDO energy, i.e., a measure of specific PRDDO error. [b] Δ_2 is the 4-31G energy relative to the STO-3G energy, i.e., a measure of the MBS error. [c] Δ_3 is the SCF-CI energy relative to the SCF energy, i.e., a measure of the differential CI stabilization.

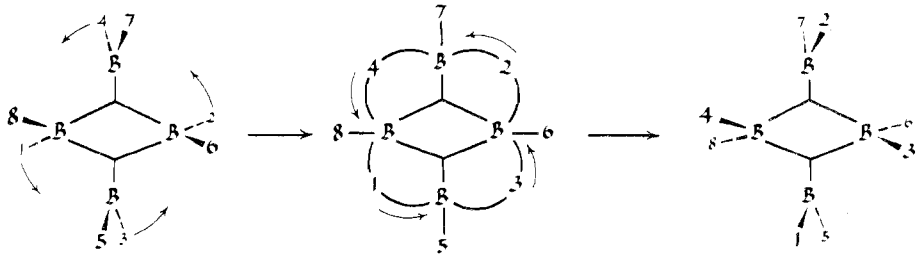

Figure 9. A possible pathway for hydrogen scrambling in 0204 ST B_4H_8 via "4020–0204A" as a candidate transition state.

Table VII. Valencies[a] and PRDDO Energies (kcal/mol)

	$V(T)^b$	$V(B)$	$V(H)$	Energy	ΔE (EC-ST)	$\Delta V(T)$ (ST-EC)	$\Delta V(B)$ (ST-EC)	$\Delta V(H)$ (ST-EC)
				B_2H_4				
2010	11.2281	7.2841	3.9440	−32 267.4				
0012 EC	9.9457	5.9728	3.9728	−32 382.3	13.2	0.1345	0.1252	0.0094
0012 ST	10.0802	6.0980	3.9822	−32 395.5				
				B_3H_7				
2102	17.5635	10.5851	6.9784	−48 934.1				
1103 EC	17.2149	10.2434	6.9715	−48 937.7	8.80	0.0907	0.0832	0.0075
1103 ST	17.3056	10.3266	6.9790	−48 946.5				
				B_4H_8				
2202B	22.6079	14.6326	7.9753	−64 743.5				
"4020"	22.4721	14.4866	7.9855	−64 744.2				
2112	21.8440	13.8655	7.9785	−64 778.8				
0204 EC	21.3275	13.3542	7.9733	−64 774.0	11.8	0.1401	0.1297	0.0104
0204 ST	21.4675	13.4838	7.9837	−64 785.8				

[a] Cf. eq 5. [b] $V(T) = V(B) + V(H)$.

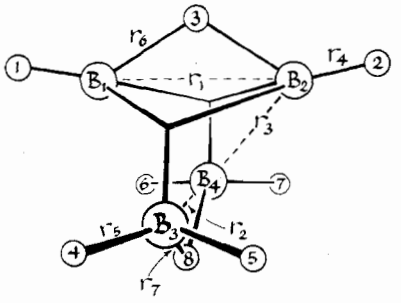

Figure 10. Optimized geometrical and Boys localized valence structure for 2202B B_4H_8: $r_1 = 2.801$ au, $r_2 = 3.717$ au, $r_3 = 3.428$ au, $r_4 = 2.177$ au, $r_5 = 2.192$ au, $r_6 = 2.531$ au, $r_7 = 2.540$ au, B_1–H_{3b}–$B_2 = 67.2°$, B_3–H_{3b}–$B_4 = 94.1°$, H_1–B_1–$H_{3b} = 108.9°$, H_4–B_3–$H_5 = 111.4°$.

MBS geometries in the more elaborate calculations of course contributes an additional uncertainty to the energy comparisons.

Valency, Strain, and Energy

The finding of vacancy structures as the most stable forms[16,27] is consistent with, though not required by, the apparently transitory nature of the unsaturated boron hydrides, as well as with their chemical behavior as ligand acceptors.[32] In view of their evident importance, we shall now consider factors which determine the relative energies of vacancy vs. nonvacancy structures, as well as the relative energies of the EC and ST conformers for the former. All structures will be included in the discussions which follow, even though only 0012 ST B_2H_4, 1103 ST (or possibly 2102) B_3H_7, and 2112C, 2202B, and 0204 ST B_4H_8 seem to represent equilibrium geometries in the absence of symmetry constraints.

Valency and Conformational Energies. For the EC, ST pairs, we found that conformational factors affect the energy by ~10–20 kcal/mol (Table V). We show in Table VII that these factors modify the overall valency in much the same way. Specifically, each additional unit of valency lowers the PRDDO energy by ~100 kcal/mol. To proceed quantitatively, we here define valency, as suggested by Armstrong, Perkins, and Stewart,[17] in terms of the degrees of bonding, B_{ab},[33] between atomic centers. Specifically, the valency of atom a, V_a, is given by

$$V_a = \sum_{a \neq b} B_{ab} = \sum_{a \neq b} \sum_{i_a} \sum_{j_b} (P_{i_a j_b})^2 \qquad (5)$$

and thus ultimately is obtained from the squares of the elements of the density matrix, **P**, over orthogonalized atomic orbitals. The sums in eq 5 extend over all orthogonalized AO's i on center a and j on center b. The total valency, V, is then the sum of the valencies of the atoms, $\sum V_a$.

Table VIII. Valency Contributions Due to Interaction of Formally Vacant Orbital i_a with Remaining Orthogonalized AO's, j_b

	$\Sigma_{j_b}(P_{i_a j_b})^2$				
	$j_b = H_t$	$j_b = H_b$	$j_b = B^a$	Total, $I_{i_a}{}^b$	ΔI^c
			B_2H_4		
0012 EC	0.0		0.0	0.0	0.1268
0012 ST	0.0336		0.0298	0.0634	(94%)[d]
			B_3H_7		
1103 EC	0.0407	0.0	0.0365	0.0772	0.0137
1103 ST	0.0424	0.0	0.0486	0.0909	(15%)[d]
			B_4H_8		
0204 EC	0.0375		0.0348	0.0723	0.0284
0204 ST	0.0392		0.0473	0.0865	(20%)[d]

[a] This column represents the contributions from orthogonalized AO's on other boron atoms. [b] $I_{i_a} = \Sigma_{j_b}(P_{i_a j_b})^2$ and represents the total contribution *per* vacant orbital i. [c] ΔI represents the difference in valency per *molecule*, ST-EC, from interactions of all the formally vacant orthogonalized AO's. [d] Percent of the change in total valency, $\Delta V(T)$, for which ΔI is responsible.

The origin of the additional valency of the ST conformers is probed in Tables VIII–X. For 0012 ST B_2H_4, 94% of the additional valency arises from terms in eq 5 which represent the increased utilization of the formally vacant orbital on boron in the wave function for the staggered conformer (Table VIII). As noted by Dill et al.,[27a] the specific interaction is hyperconjugation between the vacancy center and the π component of the (localized) molecular orbitals for the adjacent BH_2 group. No such interaction is possible in the planar EC structure.

For B_3H_7 and B_4H_8, however, the increased utilization of the formally vacant orbitals accounts for only 15–20% of the difference in valency (Table VIII). Most of the added valency of the ST conformer arises from interactions of other types between neighboring vacancy (B^v) and nonvacancy (B) borons (column 1, Table IX), partly offset by diminished interactions between pairs of nonvacancy borons and, for B_4H_8, between the vacancy borons as well (column 2). The Mulliken overlap populations (Table X) display the same features: the B^v–B bonding is stronger and the B–B and B^v–B^v bonding somewhat weaker, in the ST conformers.

The conformational changes also significantly alter the boron–hydrogen interactions (cf. Table IX). In particular, the hyperconjugative changes in the B^v–H_t contributions (both bonded and nonbonded) account for an appreciable part of the overall change in valency of the borons in B_2H_4. For B_3H_7

Table IX. Origin of Differences in Valency

$$V(\mathrm{ST}) - V(\mathrm{EC}) \equiv \sum_{a \neq b} B_{a,b}(\mathrm{ST}) - \sum_{a \neq b} B_{a,b}(\mathrm{EC})$$

	Atom pair, a–b						
			B–H_t, B^v–H_t				
	B–B^v [a]	B–B, B^v–B^v	Bonded [b]	Nonbonded [c]	B–H_b, B^v–H_b	H–H	Totals [d]
B_2H_4		+0.096	−0.077	+0.135		−0.019	0.135
B_3H_7	+0.228	−0.134	−0.179 [g] −0.029 [h]	+0.178 [g] +0.005 [h]	0.003	0.018	0.091
B_4H_8	+0.417	−0.255 [e] −0.006 [f]	−0.278 [g] −0.052 [h]	+0.267 [g] +0.011 [h]		0.038	0.140

[a] B represents a nonvacancy boron and B^v a vacancy boron. [b] H_t is attached to boron indicated. [c] H_t is not attached to boron indicated. [d] Slight inaccuracies are due to roundoff errors. [e] This value is the B–B contribution. [f] This value is the B^v–B^v contribution. [g] This contribution is from H_t's on vacancy boron. [h] This contribution is from H_t's on nonvacancy borons.

Table X. Mulliken Overlap Populations over Slater AO's

	Structures					
Boron [a]	0012 B_2H_4		1103 B_3H_7		0204 B_4H_8	
pair	EC	ST	EC	ST	EC	ST
B^v–B^v	0.807	0.876			−0.040	−0.051
B–B			0.416	0.388	0.549	0.477
B–B^v			0.372	0.430	0.354	0.405

[a] B and B^v denote nonvacancy and vacancy borons, respectively.

Table XI. Predicted (Eq 6) and Actual (PRDDO) Valencies (V) for Some Boron Hydrides [g]

Molecule	Predicted V [a]	Actual V	Diff
BH_3 [b]	6.00	5.96	−0.04
B_2H_6 [b]	13.10	13.10	0.00
B_3H_9 [c]	19.65	19.56	−0.09
B_4H_{10} [d]	24.40	24.50	+0.10
B_4H_{12} [c]	26.20	25.82	−0.38
B_5H_9 [d]	27.30	27.31	+0.01
B_5H_{11} [d]	29.05	28.99	−0.06
B_6H_{10} [e]	32.00	31.84	−0.16
B_8H_{12} [f]	41.40	41.31	−0.09

[a] $V = 2.55s + 2.70t + 2.20y + 2.00(p + x)$; cf. the discussion following eq 6. [b] Reference 5. [c] This work. Note that B_4H_{12} is severely overcrowded. [d] PRDDO-optimized geometries (I. M. Pepperberg, unpublished work) using exponents as in Table I. [e] Cf. I. R. Epstein, J. A. Tossell, E. Switkes, R. M. Stevens, and W. N. Lipscomb, *Inorg. Chem.*, **10**, 171 (1971), for geometry and exponents. [f] Cf. J. H. Hall, Jr., D. S. Marynick, and W. N. Lipscomb, *J. Am. Chem. Soc.*, **96**, 770 (1974), for geometry and exponents. [g] Rms deviation 0.15.

and B_4H_8, significant increases and decreases in valency from specific B–H interactions also occur but closely balance one another, and the overall effect is small (Table IX).

Valency and Topology. Differences in valency can also be expected to influence the relative energies of the vacancy and nonvacancy isomers for B_2H_4, B_3H_7, and B_4H_8. To examine the relationship between valency and topology, we list in Table XI valencies (PRDDO values) for six stable boron hydrides as well as for BH_3 and for the saturated transient boron hydrides B_3H_9 and B_4H_{12}. Remarkably, we find that the total valencies, V, are reproduced by the simple additive relationship

$$V = 2.55s + 2.70t + 2.20y + 2.00(p + x) \qquad (6)$$

to within an rms deviation of 0.15 (i.e., ~0.5%). Interestingly, the three-center BHB and BBB bonds represented by the *styx* numbers s and t are found to contribute more strongly to the total valency than the two-center B–B and B–H_t bonds represented by y and by $p + x$. However, the difference in valency for terminal and bridge bonds to hydrogen (0.55) is essentially the same as the difference for two- and three-center framework bonds (0.50). Thus, *styx* isomers of equal vacancy number are expected to have similar total valencies.

Table XII. Predicted and Actual Valencies for Transient Boron Hydrides [b]

	styx structure	Predicted V [a]	Actual V (PRDDO)
B_2H_4	2010	11.30	11.22
	0012	10.20	10.08 (ST)
			9.94 (EC)
B_3H_7	2102	17.80	17.56
	0104	16.70	
	1103	17.25	17.31 (ST)
			17.21 (EC)
B_4H_8	2202B	22.50	22.60
	4020	22.60	22.47
	0204A	21.40	
	2112C	22.00	21.84
	0204	21.40	21.47 (ST)
			21.33 (EC)

[a] $V = 2.55s + 2.70t + 2.20y + 2.00(p + x)$ (cf. eq 6). [b] Rms deviation 0.14.

"Actual" PRDDO valencies for B_2H_4, B_3H_7, and B_4H_8 are compared with the valencies predicted by eq 6 in Table XII. For "4020–0204A" B_4H_8 and "2102–0104" B_3H_7, the "predicted" values are for the parent $v = 0$ topologies. Also listed for comparison are the companion $v = 2$ values. The predicted and observed values again agree remarkably closely (rms deviation 0.14). Nevertheless, two trends are evident: (1) the predicted values exceed the observed valencies by 0.1–0.2 for the "$v = 0$" structures for B_3H_7 and B_4H_8; (2) for B_3H_7 and B_4H_8, the predicted valencies for each EC, ST pair closely match the EC values but underestimate the ST values by ~0.1.

Predicted and actual PRDDO valencies for individual boron atoms obtained by partitioning the total valency for each of the topological units as shown below

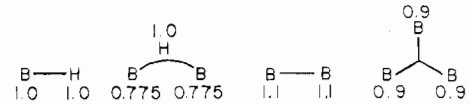

are compared in Table XIII. Except in 0012 EC B_2H_4, the actual valencies for the vacancy centers consistently exceed the predicted values, though to a greater extent in the ST than the EC conformers. Apparently, interactions which produce increased valency are also present but are less important in the EC conformers for 1103 B_3H_7 and 0204 B_4H_8. In addition, we see that the valencies for the two sets of boron atoms in "4020–0204A" B_4H_8 indeed differ qualitatively as expected from the companion $v = 2$ values, and the observed valencies for "2102–0104" B_3H_7 similarly are somewhat shaded toward the 0104 values.

Further evidence for the topologically intermediate nature of the "$v = 0$" structures is presented in Table XIV. The

Table XIII. Expected[a] vs. Actual Boron Valencies (Totals in Brackets)

	Expected V	Actual V		Expected other
		B_2H_4		
2010	3.65 (2) [7.30]	3.64 (2) [7.28]		
0012	3.0 (2) [6.0]	3.05 (2) [6.1] ST		
		2.98 (2) [5.97] EC		
		B_3H_7		
2102	3.45 (1) 3.67 (2) [10.79]	3.75 (1) 3.42 (2) [10.59]	0104	3.90 (1) 2.90 (2) [9.70]
1103	2.90 (1) 3.67 (2) [10.25]	3.06 (1) 3.63 (2) [10.32] ST		
		3.04 (1) 3.60 (2) [10.24] EC		
		B_4H_8		
2202B	3.57 (2) 3.67 (2) [14.48]	3.62 (2) 3.69 (2) [14.62]		
4020	3.65 (4)[b] [14.6]	3.42 (2) 3.82 (2) [14.48]	0204A	3.90 (2) 2.80 (2) [13.40]
2112C	3.775 (2)[c] 3.00 (1) 3.45 (1) [14.00]	3.52 (2) 3.14 (1) 3.68 (1) [13.86]		
0204	2.90 (2) 3.80 (2) [13.40]	3.05 (2) 3.69 (2) [13.48] ST		
		3.02 (2) 3.66 (2) [13.36] EC		

[a] $V = 2.55s + 2.70t + 2.20y + 2.0(p + x)$. [b] Number of equivalent atoms present. [c] This value is for a hybrid structure; that is, it is an average of the values for the two equivalent structures of 2112C topology.

observed group charges listed there were obtained from the PRDDO Mulliken atomic charge for each boron by adding the atomic charge of each attached terminal hydrogen plus half the charge of each bridge hydrogen.[34,35] Appropriately, the group charges thus sum to the net ionic charge, as do the

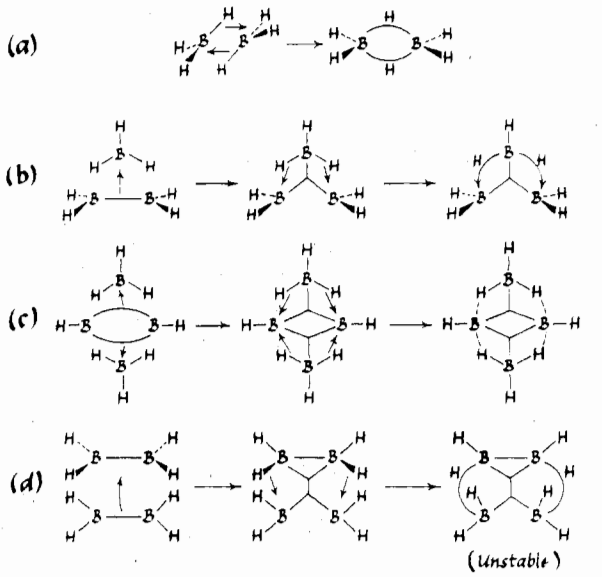

Figure 11. Illustration of interacting subunits model for some boron hydrides. Note the reciprocal donor–acceptor role played by each subunit: (a) $2BH_3 \rightarrow B_2H_6$; (b) $BH_3 + B_2H_4 \rightarrow 2102\ B_3H_7$; (c) $2BH_3 + B_2H_2 \rightarrow 4020\ B_4H_8$; (d) $2B_2H_4 \rightarrow 2112D\ B_4H_8$ (unstable).

charges assigned to boron atoms in the topological approach.[15c] For the EC and ST conformers, the self-consistent PRDDO group charges parallel the topologically predicted values but are consistently smaller. For the "$v = 0$" structures for B_3H_7 and B_4H_8, however, the qualitative pattern is not that expected for the parent 2102 and 4020 topologies but rather that expected for the companion $v = 2$ topologies, 0104 and 0204A.

Thus, the bridge hydrogen asymmetries, the charge distributions, and the total and atomic valencies are all consistent with the suggested topologically intermediate nature of the "4020–0204A" B_4H_8 and "2102–0104" B_3H_7 structures. Such a description seems quite satisfactory. Nevertheless, an alternative, but related, view is available which merits examination because it highlights an important principle of bonding in these electron-deficient compounds.

Interacting-Subunits Model. In an earlier section, we noted that both bridge bonds in B_2H_6 must form simultaneously when two BH_3 subunits are brought together (cf. Figure 11a).[5,23] Because each subunit then serves as both donor and acceptor,[23] the interaction can proceed without requiring an accumulation of electronic charge on either subunit. Similarly,

Table XIV. Group Charges

	Observed[a]					Predicted[b]			
	B1	B2	B3	B4		B1	B2	B3	B4
				B_2H_4					
2010	0.0	0.0			2010	0.0	0.0		
0012 ST	0.0	0.0			0012	0.0	0.0		
0012 EC	0.0	0.0							
				B_3H_7					
"2102–0104"	+0.040	+0.040	−0.080		2102	−0.17	−0.17	+0.34	
					0104	+0.34	+0.34	−0.67	
1103 ST	−0.078	−0.078	+0.156		1103	−0.17	−0.17	+0.34	
1103 EC	−0.065	−0.065	+0.130						
				B_4H_8					
2202B	+0.120	+0.120	−0.120	−0.120	2202B	+0.17	+0.17	−0.17	−0.17
"4020–0204A"	+0.202	+0.202	−0.202	−0.202	4020	0.0	0.0	0.0	0.0
					0204A	+0.67	+0.67	−0.67	−0.67
2112C	−0.009	+0.108	−0.049	−0.049	2112C	+0.34	+0.34	−0.34	−0.34
0204 ST	−0.159	−0.159	+0.159	+0.159	0204B	−0.34	−0.34	+0.34	+0.34
0204 EC	−0.163	−0.163	+0.163	+0.163					

[a] PRDDO values. [b] Cf. text.

Table XV. Atomization Energy, A (kcal/mol)

Structure	A(eq 10)	A(exptl)[a,b]
BH_3 (0002)	270	270
B_2H_6 (2002)	574	575
B_4H_{10} (4012)	1048	1048
B_5H_9 (4120)	1131	1130
B_5H_{11} (3203)	1227	1227
B_6H_{10} (4420)	1314	1313
$B_{10}H_{14}$ (4620)	2046	2079

[a] Cf. ref 37b. [b] These values are based on $A(B_2H_6)$ plus an estimated ΔH for dimerization of BH_3 of −35 kcal/mol: G. W. Mappes, S. A. Friedman, and T. P. Fehlner, *J. Phys. Chem.* 74, 3307 (1970).

"2102–0104" B_3H_7 and "4020–0204A" B_4H_8 can be viewed formally as arising respectively from the interaction of BH_3 subunits (v = 1) with 0012 B_2H_4 (v = 2) and with 0020 HB=BH (v = 2). Taking the donor–acceptor interactions stepwise for purposes of analysis, we see that the formation of the symmetrical BBB bond of the 0104 B_3H_7 structure (Figure 11b) lowers the total vacancy number from 3 to 2. In order to reduce the unfavorable accumulation of charge (−0.67 e) on the BH_3 subunit, some charge (∼0.33 e) then flows from each of two terminal B–H bonds into the two empty orbitals of the B_2H_4 subunit, producing the two asymmetric BHB bridges (Figure 3c). Similarly, for "4020–0204A" B_4H_8, the initial delocalization of the two B–B τ bonds of the localized HB=BH (v = 2) fragment (Figure 11c) produces the two symmetric BBB bonds of the LMO structure (Figure 8b). The unfavorable concentration of charge in the BH_3 subunits then results in the formation of the four highly asymmetric BHB bridges.

The 2112D B_4H_8 structure, which dissociated to two B_2H_4 groups upon geometry optimization, can be viewed in much the same way (Figure 11d), with one important difference: delocalization of one B–B bond into the vacant orbitals of the opposing B_2H_4 subunit yields a *four*-center BBBB bond, a structural unit which is not recognized by the topological theory and which, in the present case at least, is strongly disfavored on overlap grounds. Molecular models suggest that it is not possible to achieve, simultaneously, suitable overlap of the boron hybrids which participate in the BHB bonds and of the hybrids which would combine to form the BBBB bond.

Modest internal displacements of charge relate both idealized 2102 and 0104 molecular orbital structures for B_3H_7 to the PRDDO LMO structure shown in Figure 3b. The relationship of the 4020 structure for B_4H_8 to the PRDDO-LMO structure of Figure 8b, however, is less clear, for the B_3–B_4 bond of the 4020 structure is lost entirely.[36] This structure is perhaps best understood on the basis of the interacting-subunits model.

Valency, Topology, and Energy. We shall now examine in detail the relative stability of the vacancy and nonvacancy structures for B_2H_4, B_3H_7, and B_4H_8. It will be useful, however, to first consider the relationship between topology and energy in the better known stable boron hydrides. Following Prosen[37a] and Gunn and Green,[37b] we note that the additive bond–energy relationship

$$A = 90(p + x) + 107s + 93t + 80y \quad \text{(kcal/mol)} \tag{7}$$

predicts the experimental atomization energies, A, to within an rms deviation of ∼1 kcal/mol for the small boron hydrides listed in Table XV. The highly "resonance-stabilized" $B_{10}H_{14}$[15c,37b] is an apparent exception.

If we now rewrite eq 7 in terms of eq 6 by equating the two units of valency for each of the $p + x$ B–H_t bonds with the bond energy of 90 kcal/mol, we obtain

$$A = 45V - 8s - 28t - 19y \tag{8}$$

Table XVI. Calculated (Eq 10) and Observed (4-31G) Reaction Energies (kcal/mol)

Process	−45 ΔV	17 $\Delta s'$	28 $\Delta t'$	ΔE (eq-10)	ΔE (4-31-G)
1. $2BH_3 \rightarrow B_2H_6$ 0002 2002	−49.5	+34		−15.5	−12.2
2. $B_3H_7 \rightarrow B_3H_7$ 1103 ST 2102	−11.6	+17		+5.4	+8.1
3. $B_4H_8 \rightarrow B_4H_8$ 0204 ST "4020-0204A"	−45.0	+68		+23.0	+19.9
4. $B_4H_8 \rightarrow B_4H_8$ 0204 ST 2112C	−16.9	+34	−28	−10.9	−1.7
5. $BH_3 + B_2H_4 \rightarrow B_3H_7$ 0002 0012 ST 1103 ST	−56.2	+17	+28	−11.2	−8.2
6. $2B_2H_4 \rightarrow B_4H_8$ 0012 ST 0204 ST	−58.5		+56	−2.5	0.0

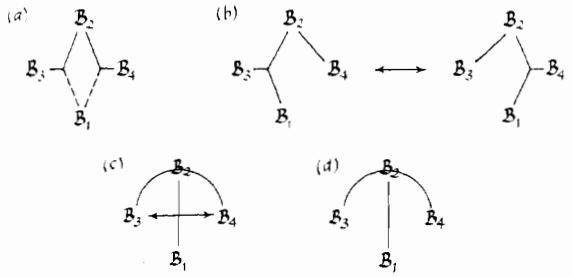

Figure 12. Alternative formulations for framework bonding on 2112C B_4H_8: (a) Boys LMO structure demonstrating apparent octet-rule violation at fractional center B_1; (b) associated hybrid representation (see text); (c) equivalent delocalized open BBB representation; (d) idealized open BBB structure.

The difference in energy expected for isomeric structures, $\Delta E \equiv E_2 - E_1 = A_1 - A_2$ (note the change in sign), thus becomes

$$\Delta E = -45V + 8\Delta s + 9\Delta t \quad \text{(kcal/mol)} \tag{9}$$

where we have used the fact that the number of framework bonds is conserved to rewrite $28\Delta t + 19\Delta y$ as $9\Delta t$. Evidently, the three-center BHB and BBB bonds are more stabilizing than their two-center counterparts (cf. eq 7), but not to the extent that their much higher valencies might suggest.

Similarly, the relative 4-31G energies for the six processes involving transient boron hydrides shown in Table XVI are reproduced to within an rms deviation of 5 kcal/mol by the simple relationship

$$E = -45V + 17\Delta s' + 28\Delta t' \quad \text{(kcal/mol)} \tag{10}$$

In most cases, the changes in the numbers of BHB and BBB bonds, $\Delta s'$ and $\Delta t'$, can equally well be determined from the LMO structures or from the *styx* numbers. For process 3 in Table XVI, however, we interpret the composite "4020–0204A" structure as having four BHB bridges plus two BBB bonds on the basis of the LMO structure (Figure 8b); thus, $\Delta s' = 4$ and $\Delta t' = 0$. In contrast, we have utilized the *styx* values for process 4, even though the LMO structure for "2112C" B_4H_8 shows two *fractional* BBB bonds. An interpretation developed in the last section of this paper (and illustrated in the comparison of parts a and b of Figure 12) supports this choice.

Strain in BHB Bridges. Like eq 9, eq 10 shows that BHB bridges and BBB bonds are less stabilizing, relative to their two-center counterparts, than their much higher valency contributions might suggest. The reason for the large difference in the coefficients of Δt and $\Delta t'$ is not clear. Interestingly, however, the difference in the coefficients of Δs and $\Delta s'$ is about that expected for the increased stabilization of a BHB bridge over a B–H_t bond by electron correlation.[38]

Moreover, indications are that the experimental or 4-31G destabilization of 8 or 17 kcal/mol per BHB bridge can be interpreted as a strain energy associated with the characteristic bent geometry adopted by BHB bridges in the polyhedral boranes. Qualitatively, the argument is that a linear geometry, usually not attainable for geometric reasons, would allow maximum overlap of the boron hybrids.[39] In order to offer a more quantitative assessment, we optimized both linear and bent geometries (B–H_b–B = 83°) for the model systems $B_2H_7^-$ and $B_2H_5^+$ in the PRDDO approximation

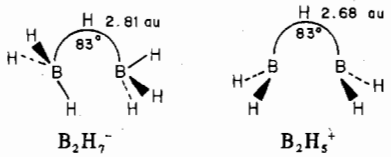

$B_2H_7^-$ $B_2H_5^+$

The eclipsed conformation shown for $B_2H_5^+$ was employed in order to minimize extraneous interactions involving the formally vacant p orbitals.

The 4-31G energies for the bent structures were found to exceed those for the optimal linear structures[40] by ~29 kcal/mol for both $B_2H_7^-$ and $B_2H_5^+$; the PRDDO destabilizations were 32 and 24 kcal/mol, respectively. In order to relate these 4-31G values to strain energies expected in polyhedral boranes, account must be taken of the additional destabilization of the bent $B_2H_7^-$ and $B_2H_5^+$ geometries arising from the Coulomb repulsion between the fractionally charged end groups. If we take the distance between the centroids of the BH_t subunits as ~4 au in the bent forms and ~6 au in the linear forms, the additional Coulombic destabilization is approximately $(0.5\ e)^2/4\ au - (0.5\ e)^2/6\ au \simeq 13$ kcal/mol. We therefore conclude that the destabilization of 17 kcal/mol in eq 10 essentially represents the 4-31G strain energy of a bent BHB bridge, as does the lower value of 8 kcal/mol in eq 9 in the context of experimental comparisons.

Strain and the Topological Rules. Finally, let us examine the relative energies for the nonvacancy 2010 B_2H_4 and 2202B B_4H_8 structures in the light of eq 10. As noted previously, 2010 B_2H_4 is topologically disallowed because both two- and three-center bonds (*two* of the latter) connect the two boron atoms. The second structure, 2202B B_4H_8, requires that two adjacent borons be connected to one another by three BBB bonds and might also be classed as topologically disallowed. As noted earlier, the B_2H_3 fragment in this structure is very similar geometrically to the B_2H_3 fragment in 2010 B_2H_4.

Equation 10 predicts that 2010 B_2H_4 should be more stable than 0012 ST B_2H_4 by $0.45 \times 1.13 - 34 \simeq 18$ kcal/mol at the 4-31G level and similarly that 2202B B_4H_8 should lie $0.45 \times 1.14 - 34 \simeq 17$ kcal/mol below the 0204 ST conformer energy. Actually, however, the two nonvacancy structures are *less* stable than their vacancy counterparts by 62 and 20 kcal/mol, respectively (Table VI). Thus, the *additional* destabilization is ~80 kcal/mol for B_2H_4 and ~37 kcal/mol for 2202B B_4H_8.

Clearly, the unfavorable bond angles around boron in both structures give rise to destabilizations much larger than those expected from eq 10 simply on the basis of the number of BHB bridges. We therefore suggest that the occurrence of three three-center bonds between a single pair of borons indeed be classed as topologically disallowed, just as is the combination of one two-center with one (or more) three-center bonds.[15] Furthermore, we infer from these comparisons that the additional destabilization due to poor overlap and geometrical strain which result from these violations of the topological rules (note that the B–B bond in 2010 B_2H_4 is required to be a π bond) is, very approximately, of the order of 50 kcal/mol.

In closing this section, we should perhaps emphasize that only a tentative analysis has been presented here. Moreover, certain aspects, e.g., the assignment of $\Delta s' = 4$ and $\Delta t' = 0$ for process 3 of Table XVI, are open to challenge. Nevertheless, we believe that the basic concept addressed here is sound, that is, that the relative energies are determined, as are the detailed geometries, principally by the interplay of opposing tendencies to maximize valency and to minimize geometrical strain. As we have seen, the intrinsic balance between the two factors is sufficiently close that vacancy structures are predicted to be the most stable for B_2H_4, B_3H_7, and B_4H_8.

Central vs. Open BBB Bonds

We shall now return to the subject of the open three-center framework bond. Based on ab initio localized-orbital studies, the open BBB bond is no longer included in the topological formalism for stable boron hydrides,[14a,15] though the open BCB bond is retained for carboranes.[10,20] The former deletion, however, provides no real justification for omitting the open three-center framework bond from the *extended* topological formalism needed to account for the transient boron hydrides.

Of the 37 topological structures which we find under the extended rules for the new B_2, B_3, and B_4 systems (Figure 1), none absolutely requires the presence of an open BBB bond. However, an open BBB bond can be substituted for a central BBB bond in 1103 B_3H_7 and in the 2112C, 2112E, 2112F, 1113A–C, and 0204B structures for B_4H_8 without violating, for example, the topological rule that prohibits neighboring borons from being connected to one another via both bridge and open three-center bonds.[15c] Five of these eight "open" structures lack even twofold symmetry and will not be considered further. Furthermore, two of the three which remain—i.e., the open structures for 1103 B_3H_7 and 0204B B_4H_8—seem incompatible both with the localization results (Figures 4 and 6) and with the absence of large barriers to interconversion of the EC and ST conformers.

For 2112C B_4H_8, however, an open structure cannot be ruled out in advance. Indeed, the failure of the Boys localization to detect an open BBB bond might simply be attributed to the known, strong preference of the Boys criterion of maximal separation of orbital centroids for equivalent-orbital descriptions.[10] The Edmiston–Ruedenberg (ER) criterion,[11,12] in contrast, is relatively free of this limitation. For example, fractional central three-center bonds appear in the Boys structure for 1,2-$C_2B_4H_6$, but the ER structure displays open BCB bonds.[10,20] Thus, the ER method can be expected to provide a more sensitive test for the suitability of an open BBB structure for 2112C B_4H_8.

For reasons of economy, we first employed the Boys LMO's for 2112C B_4H_8 as the starting set for the ER localization. For 1,2-$C_2B_4H_6$, ER localizations from starting sets of either canonical (symmetry) molecular orbitals or the Boys fractional LMO's produced identical open BCB structures. In the present case, however, the ER localization left the Boys structure essentially unchanged, and the ER and Boys LMO populations agreed to within 0.01 e. In order to counter any possible bias incurred by starting from the Boys LMO's, we then performed a second ER localization. For this localization, the starting set employed the normalized plus and minus combinations of the fractional BBB LMO's (these linear combinations resemble the open BBB bond and the associated B–B bond shown in Figure 12d) in conjunction with the remaining Boys LMO's. The results of the two ER calculations were, however, identical. Moreover, the ER second-derivative test[10] produced a distinctly negative highest eigenvalue, signifying an unambiguous localization.

Thus, the ER LMO's for 2112C B_4H_8, like the Boys LMO's, contain fractional central BBB bonds rather than an open BBB bond. Nevertheless, as we shall now show, it would be incorrect to conclude that the PRDDO wave function is incompatible with the presence of an open BBB bond. We noted

earlier that the fractional BBB LMO's produce an apparent octet rule violation at B_1 in that there are "five bonds to boron". This apparent octet rule violation can be resolved within the MO framework in either of two ways.[41] In approach 1, we begin by recognizing that the two fractional LMO's *are* fractional because they employ the same hybrid AO, say, χ_1, on center B_1. We then exploit this overutilization by multiplying out the AO expansions for the two doubly occupied fractional LMO's within the Slater determinant and striking those terms which contain $\chi_1\alpha$ or $\chi_1\beta$ twice, where α and β are the spin functions. Such terms vanish identically as a consequence of the Pauli exclusion principle. By regrouping the remaining terms, we can then reexpress the LMO wave function (Figure 12a) as the sum of the MO wave functions for the two central BBB structures shown in Figure 12b, plus other less important terms. Thus, we see that the two representations (Figure 12a and b) are essentially equivalent.

In the second approach,[41] the LMO's are transformed orthogonally so as to associate the fewest number of MO's with B_1. For 2112C B_4H_8, the transformed MO's needed for this purpose are simply the normalized plus and minus combinations of the two fractional BBB LMO's. One such combination, we find, accurately yields the expected open BBB bond. The second combination, however, produces a B_1–B_2 bond which has sufficiently large contributions from B_3 and B_4 (e.g., Mulliken populations of 0.31 e on each) for it to be classified as a four-center orbital (cf. Figure 12c).

The strong interpenetration of these multicenter orbitals essentially accounts for the fact that the ER criterion (minimum sum of exchange integrals[11,12]), like the Boys criterion, perfers the more widely separated fractional LMO's. The more important conclusion, however, is that the central and open structures of Figure 12b and c *both* correspond to the LMO structure shown in Figure 12a. Thus, the model central and open BBB formulations are not mutually exclusive but rather provide comparable first approximations to the SCF wave function. Under these geometrical conditions, which also arise in $C_2B_4H_8$, $C_2B_5H_7$, $B_{10}H_{14}$, and $B_{10}H_{14}^{2-}$,[29] the elimination of the open BBB formulation from the topological theory essentially removes an overcompleteness in the description and hence is well justified.

Acknowledgment. We wish to thank the Office of Naval Research for support of this work. We also wish to thank Dr. R. M. Stevens for many helpful discussions and for his assistance with the Slater-orbital SCF and SCF-CI calculations and Jean Evans for preparing the figures.

Appendix

The vacancy-modified *styx* rules can also be applied to predict bridge bond asymmetries and general bonding tendencies in nonvacancy stable boron hydrides. We have already shown that for the nonvacancy structures of transient B_3H_7 (2102) and B_4H_8 (4020) the charge distributions, valencies, and bridge bond asymmetries are consistent with a bonding description of these molecules in terms of an intermediate geometry between vacancy and nonvacancy valence structures. That is, by proposing averages of structures in which (1) terminal hydrogens replaced some or all of the bridges of the initial structure and (2) the boron bonding patterns were made consistent with these hydrogenic shifts, we are able to account for otherwise unexpected bonding patterns. The extension of these ideas as predictive tools for stable boron hydrides will be described in detail in a forthcoming paper;[42] however, we wish to demonstrate briefly their applicability here.

We begin by introducing the four basic criteria by which we judge the relative importance of a particular vacancy conformation. Vacancy conformations which are most like

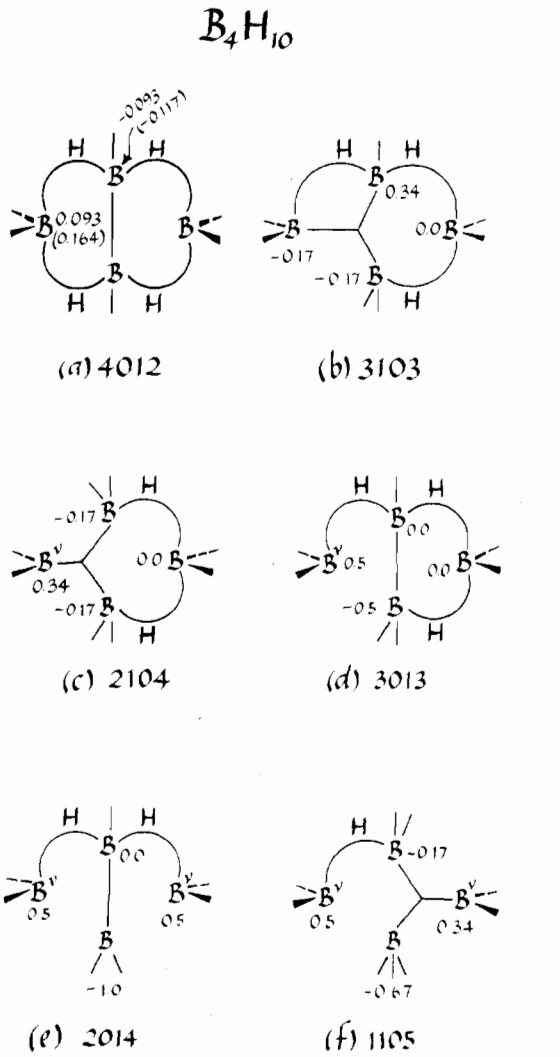

Figure 13. (a) Charges on BH_t groups and Mulliken atomic charges on boron (in parentheses) for the optimized 4012 B_4H_{10} structure. (b) Predicted charge distribution for the 3103 $v = 0$ structure for B_4H_{10}. (c)–(f) Possible B_4H_{10} structures which contain formally vacant orbitals. Each figure represents several symmetry-related structures: (c) 2104, $v = 1$; (d) 3013, $v = 1$; (e) 2014, $v = 2$; (f) 1105, $v = 2$. For these and subsequent vacancy structures, the numbers on the figures refer to the predicted charge distributions.

their stable counterparts, that is, those with (1) the fewest number of formally vacant orbitals, (2) the smallest charge separations, (3) the highest symmetries, and (4) a close adherence to the modified topological rules, would be expected to be the most important contributors to the bonding descriptions of the stable species. Structures which least correspond to their stable counterparts or which are forbidden for stable boron hydrides in the extended topological formalism (e.g., vacancy structures which contain adjacent borons unconnected by either B–B, central BBB, or BHB bonds) would be eliminated from our bonding descriptions. We will show that elimination of such structures does not affect our predictions for bridge asymmetries, charge separations, or general bonding patterns. In this context, we now examine the bonding in B_4H_{10}, B_5H_{11}, and $B_3H_8^-$.

The B_4H_{10} molecule contains four asymmetric bridge hydrogens and small but significant charges on the borons and BH_t groups[43,44] (Figure 13a). It is possible to predict this bonding pattern from a study of the several possible vacancy topologies for B_4H_{10}: four 3013 structures, two 2104 structures, two 2014 structures, and four 1105 structures (Figure 13c–f). The structures of 3013, 2014, and 1105

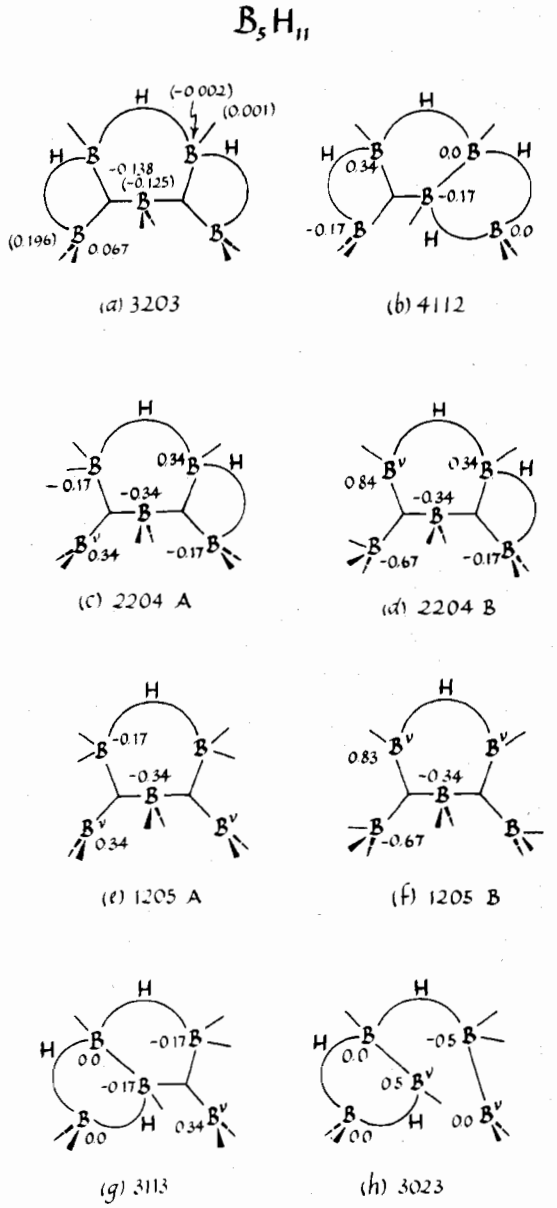

Figure 14. (a) Charges on BH_t groups and Mulliken atomic charges on boron (in parentheses) for the optimized 3203 B_5H_{11} structure. (b)–(h) Some vacancy structures for B_5H_{11}. Each figure again represents several symmetry-related structures: (b) 4112, $v = 0$; (c) 2204A, $v = 1$; (d) 2204B, $v = 1$; (e) 1205A, $v = 1$; (f) 1205B, $v = 1$; (g) 3113, $v = 1$; (h) 3023, $v = 2$.

topologies, even though they predict the proper bonding patterns,[45] fail to connect adjacent borons and are thus omitted from consideration. The 2104 topology, however, clearly satisfies all of the requirements of vacancy, charges, and topological rules. Not only do these 2104 structures predict the pattern of bridge bond asymmetry but they also predict the direction of the boron and group charge separations. This latter point demonstrates why vacancy structures are especially valuable: the 3103 nonvacancy structure[15a] (Figure 13b), which correctly predicts the direction of the bridge bond asymmetry, improperly represents the direction of the boron and group charge separations. An additional interesting feature of the 2104 topology is the three-center bond between borons that are connected only by hydrogen bridges in the 4012 nonvacancy structure. The 2104 vacancy pattern therefore predicts a certain amount of interaction of the formally "nonbonding" borons with the B–B bond of the stable structure. In fact, LMO studies have shown that the formal

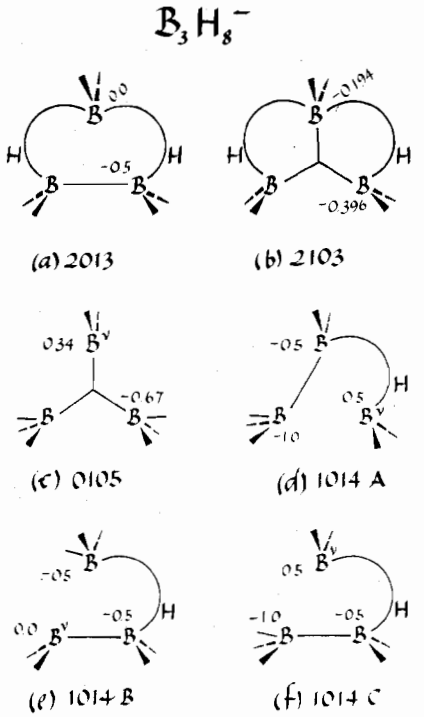

Figure 15. (a) Valence structure for the 2013 $v = 0$ $B_3H_8^-$ structure. (b) Group charges for the optimized 2103 $v = 0$ structure. (c)–(f) Possible structures for $B_3H_8^-$ which contain formally vacant orbitals: (c) 0105, $v = 1$; (d) 1014A, $v = 1$; (e) 1014B, $v = 1$; (f) 1014C, $v = 1$.

B–B bond is actually a four-center interaction which includes significant contributions (0.19 e) from each of these formally nonbonding borons.[10,44]

The ability to determine the relative contributions of each vacancy structure is important for predicting the bonding in B_5H_{11} (Figure 14)[44] because of the large number of possible vacancy structures. If all B_5H_{11} conformations contributed equally, bonding predictions would be very difficult, e.g., for the direction of bond asymmetry. However, several structures can readily be eliminated. Of the 2204A and B and 1205 A and B topologies (Figure 14c–f and symmetry-related structures), the "B" groups contribute little to the overall bonding description because of excessive charge separation.[45] Of the four additional structures, i.e., two each of 3113 and 3023 topologies (Figure 14g, h), the 3023 pair does not bond all adjacent borons and is therefore omitted. The remaining vacancy structures (2204A, 1205A, 3113) predict the bridge bond asymmetries and charge distributions actually observed in the stable B_5H_{11}. Even the bridging role of the unique H_{1t} of the apical boron in the 3113 ($v = 1$) valence configurations arises naturally. We recall that H_{1t} has been shown to exhibit some bridging characteristics, although it localizes approximately as a terminal hydrogen.[10,44,46] Interestingly, the 4112 $v = 0$ structure[15a] in which the unique H_{1t} is also a bridge cannot be used to predict the overall bonding pattern of B_5H_{11}. As noted above for the 3103 $v = 0$ B_4H_{10} structure, the nonvacancy 4112 structure fails to predict properly charge distributions (Figure 14b). One other feature of B_5H_{11} is noteworthy. The bonding between the apical boron and the BH groups has been shown in various calculations to be stronger than that between the apical boron and the BH_2 groups;[11b,44,47] the 3113 structures also predict this phenomenon. Other structures can be written which would predict some or all of the actual bonding patterns in B_5H_{11}; however, these structures are disallowed on the basis of charge separations or lack of bonds between adjacent borons.

In order to discuss $B_3H_8^-$, we introduce the vacancy-modified *styx* rules for negative ions. Thus, for a borohydride with charge c, i.e., $B_pH_{p+q}^{\ c}$, we find

$$s + x = q + c$$
$$s + t = p + c - v$$
$$t + y + q/2 = p - c$$

Since $B_3H_8^-$ is a stable anion, a 2013 valence structure (Figure 15a) for the two-bridge configuration would be predicted if we were employing the unmodified, nonvacancy *styx* rules. However, the *styx* 2103 $v = 0$ pattern (Figure 15b), which emerges from a Boys localization for the geometrically optimized structure, would not be surprising had we also investigated possible vacancy structures. Incorporation of an 0105 vacancy structure (Figure 15c) clearly demonstrates a possible origin of the observed three-center BBB bond, the bridge hydrogen asymmetries, and the relative magnitude of the group charges. Six additional 1014 structures (Figure 15d–f) are excluded because they leave adjacent borons unconnected. Thus an intermediate geometry between the 2013 and 1105 patterns predicts the observed bridge asymmetry, the magnitude of the charge separations, and the presence, and even the slight asymmetry, of the three-center BBB bond; in fact, calculations show a contribution of 0.57 e from the apical B, vs. 0.74 e from each of the basal borons, to the BBB bond.

We have therefore demonstrated that an extension of the vacancy formalism to stable boron hydrides can help predict their bonding without recourse to actual calculations. We have also shown that it is possible to make these predictions without the use of those vacancy structures which barely resemble their stable counterparts, i.e., without those having excessive charge separations, large vacancy numbers, extensive asymmetry, or unconnected adjacent centers. Although such unfavorable topologies may nevertheless contribute somewhat to the overall bonding description, they are not necessary to achieve qualitatively the correct bonding predictions.

Registry No. BH_3, 13283-31-3; B_2H_4, 18099-45-1; B_3H_7, 12429-70-8; B_3H_9, 36350-66-0; B_4H_8, 12007-71-5; B_4H_{12}, 60349-62-4.

References and Notes

(1) For convenience, the abbreviations used in this paper are collected here: STO, Slater-type orbital; 3G, three Gaussian functions per STO; the numbers *styx* refer to bridge hydrogens (s), three-center bonds (t), single B–B bonds (y), and extra BH or BH_2 groups (x); MBS, minimum basis set; SCF here refers only to MBS-STO results in which all integrals are accurate; CI, configuration interaction; 4-31G refers to the extended basis set consisting of 4 Gaussian inner shell atomic orbitals and valence orbitals split into 3 Gaussian inner and 1 Gaussian outer parts; ER, Edmiston–Ruedenberg criteria for localizing molecular orbitals; ST, staggered conformation; EC, eclipsed conformation; LST, linear synchronous transit; PRDDO, partial retention of diatomic differential overlap; LMO, localized molecular orbital; A, experimental energy of atomization; V, valency as defined in the paragraph containing eq 5; AO, atomic orbital; $B_pH_{p+q}^{\ c}$ refers to a boron hydride with charge c containing p borons and $p + q$ hydrogens.

(2) (a) Harvard University. (b) City University of New York.

(3) We define an unsaturated hydride as one which contains a vacant orbital.

(4) Cf. discussions by (a) T. P. Fehlner in "Boron Hydride Chemistry", E. L. Muetterties, Ed., Academic Press, New York, N.Y., 1975, pp 185–186, and references therein; (b) N. N. Greenwood in "Comprehensive Inorganic Chemistry", J. C. Bailar, H. J. Emeleus, R. Nyholm, and A. F. Trotman-Dickenson, Ed., Pergamon Press, Oxford, 1973, pp 769–773.

(5) D. A. Dixon, I. M. Pepperberg, and W. N. Lipscomb, *J. Am. Chem. Soc.*, **96**, 1325 (1974), and references therein.

(6) W. N. Lipscomb, "Boron Hydrides", W. A. Benjamin, New York, N.Y., 1963, pp 176–179.

(7) T. A. Halgren and W. N. Lipscomb, *Proc. Natl. Acad. Sci. U.S.A.*, **69**, 652 (1972); T. A. Halgren and W. N. Lipscomb, *J. Chem. Phys.*, **58**, 1569 (1973).

(8) W. J. Hehre, R. F. Stewart, and J. A. Pople, *J. Chem. Phys.*, **51**, 2657 (1969); W. J. Hehre, R. Ditchfield, R. F. Stewart, and J. A. Pople, *ibid.*, **52**, 2769 (1970); R. Ditchfield, W. J. Hehre, and J. A Pople, *ibid.*, **54**, 724 (1971); W. J. Hehre and W. A. Lathan, *ibid.*, **56**, 5255 (1972).

(9) R. M. Stevens, *J. Chem. Phys.*, **52**, 1397 (1970).

(10) D. A. Kleier, T. A. Halgren, J. H. Hall, Jr., and W. N. Lipscomb, *J. Chem. Phys.*, **61**, 3905 (1974), and references therein. The Boys criterion is presented and discussed by S. F. Boys in "Quantum Theory of Atoms, Molecules, and the Solid State", P. O. Lowdin, Ed., Academic Press, New York, N.Y., 1966, p 253.

(11) (a) E. Switkes, R. M. Stevens, W. N. Lipscomb, and M. D. Newton, *J. Chem. Phys.*, **51**, 2085 (1969); (b) E. Switkes, W. N. Lipscomb, and M. D. Newton, *J. Am. Chem. Soc.*, **92**, 3847 (1970); (c) M. D. Newton, E. Switkes, and W. N. Lipscomb, *J. Chem. Phys.*, **53**, 2645 (1970); (d) M. D. Newton and E. Switkes, *ibid.*, **54**, 3179 (1971).

(12) C. Edmiston and K. Ruedenberg, *Rev. Mod. Phys.*, **35**, 457 (1963).

(13) Although we will not discuss borane in detail, the extended formalism described herein will, of course, apply.

(14) (a) Reference 6, pp 43–53; (b) W. H. Eberhardt, B. C. Crawford, Jr., and W. N. Lipscomb, *J. Chem. Phys.*, **22**, 989 (1954).

(15) (a) Reference 6, pp 53–78; (b) R. E. Dickerson and W. N. Lipscomb, *J. Chem. Phys.*, **27**, 212 (1957); (c) I. R. Epstein and W. N. Lipscomb, *Inorg. Chem.*, **10**, 1921 (1971), and references therein; (d) S. Leibowitz, I. R. Epstein, and D. J. Kleitman, *J. Am. Chem. Soc.*, **96**, 2704 (1974), and references therein.

(16) J. A. Dupont and R. Shaeffer, *J. Inorg. Nucl. Chem.*, **15**, 310 (1960).

(17) D. R. Armstrong, P. G. Perkins, and J. J. P. Stewart, *J. Chem. Soc., Dalton Trans.*, 838 (1973).

(18) W. N. Lipscomb, *J. Phys. Chem.*, **62**, 381 (1958).

(19) D. S. Marynick and W. N. Lipscomb, *J. Am. Chem. Soc.*, **94**, 8699 (1972).

(20) I. R. Epstein, D. S. Marynick, and W. N. Lipscomb, *J. Am. Chem. Soc.*, **95**, 1760 (1973), and references therein.

(21) We note that while fivefold coordination is sometimes required (e.g., B_5H_9), it occurs only for fractional centers. Five full bonds to boron are not topologically allowed.

(22) So far, where symmetry is absent, as in $B_{16}H_{20}$, the structure arises from a compatible fusion of smaller, symmetric fragments: D. A. Dixon, D. A. Kleier, T. A. Halgren, and W. N. Lipscomb, *J. Am. Chem. Soc.*, **98**, 2086 (1976). For molecules such as $B_{10}H_{13}^-$, where x-ray studies have shown symmetry to be absent from the solid state [L. G. Sneddon, J. C. Huffman, R. Schaeffer, and W. E. Streib, *Chem. Commun.*, 474 (1972)], NMR spectra provide evidence for the existence of a symmetric structure in solution [A. R. Siedle, G. M. Bodner, and L. J. Todd, *J. Inorg. Nucl. Chem.*, **33**, 3671 (1971)].

(23) C. Edmiston and P. Linder, *Int. J. Quantum Chem.*, **7**, 309 (1973).

(24) I. M. Pepperberg, T. A. Halgren, and W. N. Lipscomb, *J. Am. Chem. Soc.*, **98**, 3442 (1976).

(25) T. A. Halgren, I. M. Pepperberg, and W. N. Lipscomb, unpublished results.

(26) (a) T. A. Halgren, I. M. Pepperberg, and W. N. Lipscomb, *J. Am. Chem. Soc.*, **97**, 1248 (1975); (b) T. A. Halgren, W. N. Lipscomb, to be submitted for publication; (c) T. A. Halgren, work in progress.

(27) This assessment has been confirmed elsewhere: (a) 6-31G*, J. Dill, P. v. R. Schleyer, and J. A. Pople, *J. Am. Chem. Soc.*, **97**, 3402 (1975); these authors find the staggered form to be the more stable by 10.5 kcal/mol; (b) FSGO, P. H. Bulstin and J. W. Linnett, *J. Chem. Soc., Faraday Trans. 2*, **71**, 1058 (1975); the staggered form is found to be 1.9 kcal/mol more stable than the eclipsed form; (c) D. R. Armstrong, *Inorg. Chim. Acta*, **18**, 13 (1976); the ST form of 1103 B_3H_7 is found to be ~18 kcal/mol more stable than the EC for unoptimized EC.

(28) This occurred even though bridge exponents were used throughout the optimization.

(29) W. N. Lipscomb, *Acc. Chem. Res.*, **6**, 257 (1973), and references therein.

(30) Further refinements using terminal exponents (Table II) for the weakly bridging hydrogens produced little change in geometry but did lower the energy ~10 kcal/mol (cf. Table V). PRDDO favors somewhat smaller hydrogen exponents and larger boron exponents than those which are obtained in ab initio SCF optimization using the method of Stevens.[9]

(31) Orthogonal optimization of 4020 as a candidate transition state (cf. ref 26a, b) for either process would impose no symmetry restrictions and would result in a refined transition state of somewhat lower energy.

(32) Experimental observations also suggest the existence of such species: (a) R. T. Paine, G. Sodek, and F. E. Stafford, *Inorg. Chem.*, **9**, 877 (1970); (b) R. E. Hollins and F. E. Stafford, *ibid.*, **11**, 2593 (1972); (c) ref 4b, pp 785–786, 791; (d) J. D. Glore, J. W. Rathke, and R. Shaeffer, *Inorg. Chem.*, **12**, 2175 (1973); (e) J. W. Rathke and R. Shaeffer, *ibid.*, **13**, 760 (1974); (f) E. J. Stampf, A. R. Garber, J. D. Odom, and P. D. Ellis, *ibid.*, **14**, 2446 (1975).

(33) K. Wiberg, *Tetrahedron*, **24**, 1083 (1968); (b) C. Trindle, *J. Am. Chem. Soc.*, **91**, 219 (1969).

(34) J. H. Hall, Jr., D. A. Dixon, D. A. Kleier, T. A. Halgren, L. D. Brown, and W. N. Lipscomb, *J. Am. Chem. Soc.*, **97**, 4202 (1975).

(35) For the asymmetric bridges, the atomic charge on hydrogen is sufficiently small (≤0.04 in magnitude) that an asymmetric rather than a symmetric division of charge would make little difference.

(36) Moreover, the residual B_3–B_4 interaction is appropriately repulsive; the PRDDO Mulliken overlap population is −0.08 e.

(37) (a) E. J. Prosen, paper presented at the Symposium on Hydrides, 127th National Meeting of the American Chemical Society, Cincinnati, Ohio, 1955; see Abstracts, p 30Q; cf. S. H. Bauer, *J. Am. Chem. Soc.*, **80**, 294 (1958); (b) S. R. Gunn and L. G. Green, *J. Phys. Chem.*, **65**, 2173 (1961).

(38) M. Gelus, R. Ahlrichs, V. Staemmler, and W. Kutzelnigg, *Chem. Phys. Lett.*, **7**, 503 (1970).

(39) A nonlinear BHB bond is energetically unfavorable because the orbitals involved are unable to achieve maximum overlap. Cancelations involving the negative lobes of the boron sp^x hybrids used in bonding reduce the overlap progressively as the B–H_b–B angle increases. Similar cancelations

occur in the τ bond representation for the double bond of ethylene; and consequently the C–C double bond is not twice as strong as a C–C single bond.
(40) Ab initio calculations have found that the linear form of $B_2H_7^-$ is the most stable: J. H. Hall, Jr., D. S. Marynick, and W. N. Lipscomb, *Inorg. Chem.*, **11**, 3126 (1972).
(41) T. A. Halgren, L. D. Brown, D. A. Kleier, and W. N. Lipscomb, submitted for publication.
(42) I. M. Pepperberg and W. N. Lipscomb, in preparation.
(43) We report both group charges and atomic charges, although the former are more suitable for comparison with the predicted charges (cf. text). For $B_3H_8^-$, the borons are actually all positive, so that the group charges are the only ones applicable for comparison.
(44) I. M. Pepperberg, unpublished results.
(45) Note that the group charge separations predicted by the two 2014 structures, for example, are not −1.0, 0.0, +0.5, +0.5, but rather −0.5, −0.5, +0.5, +0.5, that is, an *average* of the predictions for the two structures of the same topology. For the 2204B and 1205B B_5H_{11} structures, even the averaged charge separations are too large for these structures to be important.
(46) R. Schaeffer and J. C. Huffman, private communication; J. C. Huffman, Ph.D. Thesis, Indiana University, 1974.
(47) E. Switkes, I. R. Epstein, J. A. Tossell, R. M. Stevens, and W. N. Lipscomb, *J. Am. Chem. Soc.*, **92**, 3837 (1970).

Contribution from the Department of Chemistry,
University of Southern California, Los Angeles, California 90007

Methoxytrifluoromethylphosphines and Their Borane(3) Complexes

ANTON B. BURG

Received July 14, 1976 AIC60514G

New phosphines of the prototype $CH_3O(CF_3)PX$ have been made, starting with $CH_3O(CF_3)PCl$, formed (91%) from $(CH_3O)_2PCF_3$ and CF_3PCl_2, catalyzed by $(CH_3)_3N$. NaI converts $CH_3O(CF_3)PCl$ to $CH_3O(CF_3)PI$, which Hg converts to the diphosphine $(CH_3OPCF_3)_2$. From this comes $CH_3O(CF_3)PH$ by action of CH_3OH; and $CH_3O(CF_3)PF$ is made from $(CH_3O)_2PCF_3$ by action of BF_3 at oxygen. However, BF_3 does not attack the second oxygen; CF_3PF_2 is not formed. The diphosphine $(CH_3OPCF_3)_2$ is cleaved by HCl or BF_3, which seems to attack at oxygen; the major result is disproportionation to $(CH_3O)_2PCF_3$ and $(CF_3P)_n$ or secondary products. A probable CF_3HPCl was a minor product of the HCl reaction. The BH_3 complexes of some of these phosphines were found to be of the relatively volatile, nonpolar type, with too little hydridic character for reaction with HCl to make H_2; and they are far more stable than the classical examples of this type, $BH_3{\cdot}CO$ and $BH_3{\cdot}PF_3$. Both $(CH_3OPCF_3)_2{\cdot}BH_3$ and $(CH_3OPCF_3)_2{\cdot}2BH_3$ equilibrate with diborane and their predecessors; apparently the second BH_3 is bonded no less effectively than the first. Infrared spectra are listed, including evidence that P–H bonding is stronger in $CH_3O(CF_3)PH{\cdot}BH_3$ than in the free phosphine. Characterization by NMR spectra also is extensive.

Fluorocarbon phosphines having alkoxy groups on phosphorus are potentially interesting ligands for the fuller study of complexes in which bases act both as σ donors and as π acceptors. It is now well understood that a CF_3 group enhances the π-acceptor action of phosphorus, while suppressing its σ-donor bonding power, whereas a methoxy group improves the σ-donor action of phosphorus while competing with π return bonding by the Lewis acid or metal atom. There might be situations such that the attachment of both groups to phosphorus would lead to unexpectedly strong ligation. However, very few alkoxyfluorocarbon phosphines have been reported. The present study develops especially the type $CH_3O(CF_3)PX$.

The ligand character of these new phosphines was explored by studying their BH_3 complexes. In general, BH_3 complexes have divided sharply into two classes: the highly polar, rapidly formed, and strongly hydridic base-donor type such as $(CH_3)_3N{\cdot}BH_3$, $(CH_3)_3P{\cdot}BH_3$, or the far less stable $(CH_3)_2O{\cdot}BH_3$; and the virtually nonpolar, slowly formed, and essentially nonhydridic type exemplified by $BH_3{\cdot}CO$, $BH_3{\cdot}PF_3$, or $BH_3{\cdot}P(OCH_3)_3$, wherein the polarity expected from base-donor action is neutralized by a π-type return of B–H bonding electrons in the manner of hyperconjugation. As mentioned in a plenary lecture some years ago,[1] the hydridic character of the base-donor class is demonstrated by rapid reaction with HCl to form hydrogen and place Cl on B, whereas the donor-acceptor class seems to be inert toward HCl except in the sense that HCl attacks the BH_3 group as it is liberated by dissociation of the complex.

The $CH_3O(CF_3)PX{\cdot}BH_3$ complexes conform to the latter class, for they form slowly, are highly volatile relative to their molecular weights, and react with HCl only at rates corresponding to their dissociation. However, they are far more stable than $BH_3{\cdot}CO$ or $BH_3{\cdot}PF_3$, presumably because of the base-enhancement effect of the methoxy group on phosphorus.[2] It seems clear, then, that the study of transition element complexes of the $CH_3O(CF_3)PX$ phosphines would be interesting because both their σ-donor and π-acceptor bonding would be strong.

Experimental Methods

The present studies were performed by means of a Stock-type high-vacuum manifold, with mercury float-valves for quantitative work with volatile compounds or with Apiezon L greased stopcocks where suitable. Infrared spectra were recorded accurately by the Beckman IR7 instrument with NaCl or CsI optics or, for quick identification, by the Beckman IR20A. The frequencies are reported in cm^{-1} with relative intensities in parentheses, calculated by the equation $k = (100/PL) \log (I_0/I)$ for pressure P and path L both in cm.

Preliminary NMR spectra were recorded for ^1H or ^{19}F by the Varian T-60 instrument, but for higher accuracy and sensitivity the Varian XL-100-FT instrument was used. For ^{13}C spectra, each sample was in a 12-mm thin-wall tube with a concentric 5-mm tube containing C_6D_6, which served as the lock and chemical shift standard. For the other nuclei, the samples usually were in 1-mm i.d. microtubes, concentrically placed in 5-mm thin-wall tubes containing the acetone-d_6 or benzene-d_6 lock standard. For the chemical shifts, the standard offsets for TMS, Cl_3CF, H_3PO_4, or $(CH_3O)_3B$ were determined with similar microsamples, minimizing the effects of diamagnetic differences. For all chemical shifts, the positive direction is upfield, including the τ values for protons, defined as the distance upfield from TMS − 10 ppm. The coupling constants J are in s^{-1} ("Hz").

The Monophosphines

Methoxytrifluoromethylphosphine. The compound $CH_3O(CF_3)PH$ was first recognized as a minor product of the methanolysis of $(CF_3P)_4$.[3] A more convenient, virtually quantitative synthesis was performed by methanol cleavage of the diphosphine $(CH_3OPCF_3)_2$ (described later), according to the millimole stoichiometry

$$\underset{0.352}{(CH_3OPCF_3)_2} + \underset{0.352}{CH_3OH} \rightarrow \underset{0.372}{(CH_3O)_2PCF_3} + \underset{0.312}{CH_3O(CF_3)PH} \quad (1)$$

This reaction occurred in a small U-tube between mercury float-valves, during slow warming from −78 to +50 °C. The